

CERN-TH/2001-306

DESY 01-206

hep-ph/0112161

Transplanckian Collisions at the LHC and Beyond

Gian F. Giudice^a, Riccardo Rattazzi^{a†}, James D. Wells^{b,c}

^(a) *CERN, Theory Division, CH-1211 Geneva 23, Switzerland*

^(b) *Physics Department, University of California, Davis, CA 95616, USA*

^(c) *Deutsches Elektronen-Synchrotron DESY, D-22603 Hamburg, Germany*

Abstract

Elastic collisions in the transplanckian region, where the center-of-mass energy is much larger than the fundamental gravity mass scale, can be described by linearized general relativity and known quantum-mechanical effects as long as the momentum transfer of the process is sufficiently small. For larger momentum transfer, non-linear gravitational effects become important and, although a computation is lacking, black-hole formation is expected to dominate the dynamics. We discuss how elastic transplanckian collisions can be used at high-energy colliders to study, in a quantitative and model-independent way, theories in which gravity propagates in flat extra dimensions. At LHC energies, however, incalculable quantum-gravity contributions may significantly affect the experimental signal.

December 2001

[†]On leave of absence from INFN, Pisa.

Contents

1	Introduction	2
2	Scattering in the Eikonal Approximation	7
2.1	The Eikonal Amplitude	7
2.2	Cross Sections	13
2.3	Physical Interpretation	14
2.4	Corrections to the Eikonal Approximation	17
2.5	Quantum-Gravity Effects	21
3	Phenomenology in the Transplanckian Regime	28
3.1	Signals at the LHC	28
3.2	Other Future Colliders	37
3.3	Comparison among Gravity Signals at the LHC	40

1 Introduction

The hypothesis that the characteristic energy scale of quantum gravity lies just beyond the electroweak scale finds its motivation in the hierarchy problem and its operative realization in the existence of extra spatial dimensions [1, 2]. If this hypothesis is verified in nature, future experiments at the LHC have the ground-breaking opportunity of testing the dynamics of gravitation in the high-energy and quantum regimes. Unfortunately, since quantum-gravity dynamics are still unknown, systematic theoretical predictions cannot be made. It is then important to identify certain collider topologies and kinematical regions that allow a description based only upon general principles and not on model peculiarities, and which can be used in the experimental program as a handle to demonstrate the gravitational nature of the interaction. Single graviton emissions satisfy these requirements and allow for a model-independent study of the propagation of gravitational forces in extra spatial dimensions [3, 4]. On the other hand, model-dependent experimental signals, as those originating from contact interactions [3, 5] or, more likely, the observation of a specific spectrum of string Regge excitations [6] will be very important to discriminate among various models and to guide theoretical research.

The model-independent experimental signals discussed in refs. [3, 4] are based upon interactions at energies below the quantum gravity scale M_D (the analogue of the Planck mass for a D -dimensional theory), and their theoretical description fails as we approach M_D . However, there is another kinematical regime that can be tackled in a fairly model-independent fashion: the transplanckian region $\sqrt{s} \gg M_D$. This is the subject of this paper. A peculiarity of hadron machines is that, because of the composite structure of the proton, one can study, in the same environment, parton collisions at different center-of-mass energies. Consequently, if $M_D \simeq \text{TeV}$ experiments at the LHC could probe the cisplanckian (graviton emission, contact interactions), the planckian (the core of the quantum-gravity dynamics), and the transplanckian regions.

To understand the nature of transplanckian collisions, we first identify the relevant scales. Let us consider general relativity in $D = 4 + n$ dimensions with (generalized) Newton's

constant G_D . For n flat dimensions compactified in a volume V_n , G_D is related to the usual Newton's constant by $G_D = V_n G_N$. To better elucidate the relation between the transplanckian and the classical limit, we reinstate for a moment the correct powers of \hbar and c . The relation between G_D and the D -dimensional Planck scale is

$$G_D = \frac{(2\pi)^{n-1} \hbar^{n+1}}{4c^{n-1} M_D^{n+2}}, \quad (1)$$

where the proportionality constant follows from the conventions of ref. [3]. Notice that G_D has dimensions $[G_D] = \ell^{n+5} E^{-1} t^{-4}$ (ℓ = length, E = energy, t = time). Starting from G_D , we can construct the Planck length

$$\lambda_P = \left(\frac{G_D \hbar}{c^3} \right)^{\frac{1}{n+2}}. \quad (2)$$

This is the distance below which quantum gravity effects become important.

Using the center-of-mass energy of the collision, we can construct the length

$$\lambda_B = \frac{4\pi \hbar c}{\sqrt{s}}. \quad (3)$$

This is the de Broglie wavelength of the colliding particles, which characterizes their quantum length scale.

Combining G_D and \sqrt{s} , we can form the Schwarzschild radius of a system with center-of-mass energy \sqrt{s} [7]

$$R_S = \frac{1}{\sqrt{\pi}} \left[\frac{8\Gamma\left(\frac{n+3}{2}\right)}{(n+2)} \right]^{\frac{1}{n+1}} \left(\frac{G_D \sqrt{s}}{c^4} \right)^{\frac{1}{n+1}}. \quad (4)$$

This is the length at which curvature effects become significant. In the limit $\hbar \rightarrow 0$, with G_D and \sqrt{s} fixed, M_D vanishes, showing that classical physics correspond to transplanckian (macroscopically large) energies. Moreover, in the same limit, R_S remains finite, while the two length scales λ_P and λ_B go to zero. Therefore, the transplanckian regime corresponds to a classical limit in which the length scale R_S characterizes the dynamics,

$$\sqrt{s} \gg M_D \quad \Rightarrow \quad R_S \gg \lambda_P \gg \lambda_B. \quad (5)$$

For instance, by simple dimensional analysis and analyticity in G_D , we expect that the scattering angle for a collision with impact parameter b is $\theta \sim G_D \sqrt{s}/b^{n+1} = (R_S/b)^{n+1}$. This behavior shows that by increasing the energy we can obtain a finite angle scattering by going to larger b , and therefore further suppressing short distance quantum gravity effects.

This property of gravity should be contrasted to what happens in an ordinary gauge theory, where spin-1 particles mediate the force. In $(4+n)$ -dimensional space-time the gauge coupling e^2 has dimension $[e^2] = \ell^{n+1}E$. The analogues of M_D , λ_P and R_S are given respectively by $M_e^n = (\hbar c)^{n+1}/e^2$, $\lambda_e^n = e^2/(\hbar c)$ and $R_e^{n+1} = e^2/\sqrt{s}$. In the $\hbar \rightarrow 0$ limit, with e^2 and \sqrt{s} fixed, we find that $\lambda_e \rightarrow \infty$ (we focus for simplicity on $n > 0$) indicating that quantum fluctuations are not suppressed at any finite length. Indeed the same dimensional argument we used before gives a classical scattering angle $\theta \sim e^2/(\sqrt{s}b^{n+1})$, which remains finite as $\sqrt{s} \rightarrow \infty$ provided $b \rightarrow 0$. But $b < \lambda_e$ is the regime where quantum effects are unsuppressed, so we conclude that there is no classical limit. The different properties of spin-2 and spin-1 exchange that are elucidated by this simple dimensional analysis are the same that render the eikonal approximation consistent for the first and inconsistent for the second. Basically it is because energy itself plays the role of charge in gravity: when the energy is large, gravity gives sizeable effects also at large distance where quantum fluctuations of the geometry are irrelevant.

Having established that scattering at transplanckian energies is described by classical physics, one also realizes that the corresponding amplitude should only be calculable by a non-perturbative approach. This is always the case for semiclassical amplitudes (like instantons for example), for which the classical action S is much larger than \hbar , and we cannot perturbatively expand $\exp(-S/\hbar)$. In order to tackle the non-perturbative problem, we will further restrict the range of distance scales under investigation, and only consider collisions with impact parameter b much larger than R_S . In this regime, the curvature is small, the metric is nearly flat, and we can work in the limit of weak gravitational field, neglecting non-linear effects of the graviton couplings. The non-perturbative interactions between the high-energy colliding partons and the weak gravitational field can be computed using the eikonal approximation, which can be trusted at small scattering angle. From a

field-theoretical point of view, this approximation corresponds [8] to a resummation of an infinite set of Feynman diagrams which, at each order in perturbation theory, give the leading contributions to the forward scattering. The eikonal approximation has been employed for 4-dimensional gravity [9] and for string theory [10, 11] (see also ref. [12]). The results for the scattering amplitude agree with those obtained [13] by solving the Klein-Gordon equation for a particle propagating in the classical gravitational shock wave produced by the other particle [14], or by reformulating quantum gravity as a topological field theory [15]. All these different approaches give equivalent results [9, 16].

In sect. 2 we will derive and discuss the scattering amplitude in the eikonal approximation for 4-dimensional colliding particles (living on a 3-brane) and D -dimensional gravity [17] (see also ref. [18]). As explained above, the process is essentially classical, like the motion of two (relativistic) stars coming within a close distance. However, an important difference is that the gravitational potential in the non-relativistic analogue of our process decreases with the distance r as $V(r) \propto G_D/r^{n+1}$. As discussed in sect. 2 this will have significant consequences, and it will lead to quite different results from the case of 4-dimensional Newtonian potentials. A novel feature is the emergence of a new length scale

$$b_c \propto \left(\frac{G_D s}{\hbar c^5} \right)^{\frac{1}{n}}. \quad (6)$$

Notice that b_c cannot be defined in 4 dimensions ($n = 0$). In the limit $\hbar \rightarrow 0$, we find that b_c goes to infinity and therefore the classical region extends only up to length scales of order b_c . For impact parameters larger than b_c , the process is no longer determined by classical properties. However, since quantum gravity effects are always negligible, ordinary relativistic quantum mechanics is sufficient to compute scattering amplitudes within our approximation.

As previously discussed, we are limited by our computational ability to work at $b \gg R_S$. As the impact parameter approaches the Schwarzschild radius (and our expressions become unreliable), we expect to enter a (classical) regime in which the gravitational field is strong, non-linear effects are important and, plausibly, black holes are formed. This regime, discussed in ref. [19] (see also ref. [20]), is very exciting from the experimental point of view, but more arduous from a theoretical point of view. While in the eikonal region we are able to make

quantitatively reliable predictions with controllable expansion parameters, the black-hole production cross section can only be estimated with dimensional arguments and more precise information should wait for numerical simulations in D -dimensional general relativity.

Black-hole production results in a black disk of radius R_S in the cross section, since any initial state with $b < R_S$ is absorbed by the black hole (this point of view has been criticized in ref. [21]). Collisions with an impact parameter b smaller than the Schwarzschild radius do not directly probe physics at the energy scale $1/b$. Ultraviolet dynamics and quantum effects are screened by the black hole.

The physical picture we have been describing holds if there is a clear separation of the various length scales and if no other new dynamics intervene at distances between R_S and b_c . As we will discuss in this paper, this is not necessarily the case for particle collisions at the LHC. Given the present lower limits on M_D , the center-of-mass energy at the LHC can be only marginally in the transplanckian region, and a clear separation between the quantum-gravity scale λ_P and the classical scale R_S is not completely achieved, endangering our approximations. The problem is particularly apparent in string theory, which contains a new scale, the string length

$$\lambda_S = \sqrt{\alpha'}, \quad (7)$$

where α' is the string tension. In weakly-coupled string theory, λ_S is larger than λ_P and string effects can set in and modify gravity in an intermediate regime between the eikonal elastic scattering and black-hole formation. These are interesting effects, as the LHC can directly probe the nature of string theory [22]. However, model-independent calculability of the elastic channel is lost. In this paper we will consider only the pure transplanckian gravitational scattering, assuming that quantum-gravity effects are small.

The relevance of our considerations for experiments at the LHC and other future colliders is discussed in sect. 3. We will compute the elastic cross section in the transplanckian eikonal regime,

$$M_D/\sqrt{s} \ll 1, \quad -t/s \ll 1, \quad (8)$$

where t is the Lorentz-invariant Mandelstam variable, and $-t/s$ is a measure of the scattering

angle in the center-of-mass frame. The experimental signal will be discussed and compared with the expected Standard Model (SM) rate and with black-hole production.

2 Scattering in the Eikonal Approximation

2.1 The Eikonal Amplitude

We are interested in the elastic scattering of two massless 4-dimensional particles (living on a 3-brane) due to a D -dimensional weak gravitational field in the kinematic limit of eq. (8). We will focus on the case in which the two colliding particles are different, but the case of identical particles is analogous. In the eikonal approximation, we consider the infinite set of ladder and cross-ladder Feynman diagrams which give the leading contribution to forward scattering.

Since we are working in the approximation of small momentum transfer, we can compute the coupling between the colliding particle Φ and the small fluctuation around the flat metric (the graviton), taking Φ to be on-shell:

$$\frac{1}{M_D^{1+n/2}} \langle \Phi(p) | T^{\mu\nu} | \Phi(p) \rangle = \frac{2p^\mu p^\nu}{M_D^{1+n/2}}. \quad (9)$$

Here $T^{\mu\nu}$ is the energy-momentum tensor and p^μ is the 4-momentum of the particle Φ . Notice that eq. (9) is equally valid for colliding particles of any spin.

In the Φ propagators we keep only the leading terms in the momentum transfer q :

$$\begin{aligned} \frac{i}{(p+q)^2} &\rightarrow \frac{i}{2pq} \quad \text{for bosons,} \\ \frac{i}{\not{p} + \not{q}} &\rightarrow \frac{i|\Phi(p)\rangle\langle\Phi(p)|}{2pq} \quad \text{for fermions.} \end{aligned} \quad (10)$$

Since the factor $\not{p} = |\Phi(p)\rangle\langle\Phi(p)|$ in eq. (10) is used to reconstruct the on-shell vertices of eq. (9) in the ladder diagrams, we observe that not only the interaction vertices but also the propagators of bosons and fermions are identical in the eikonal approximation. This

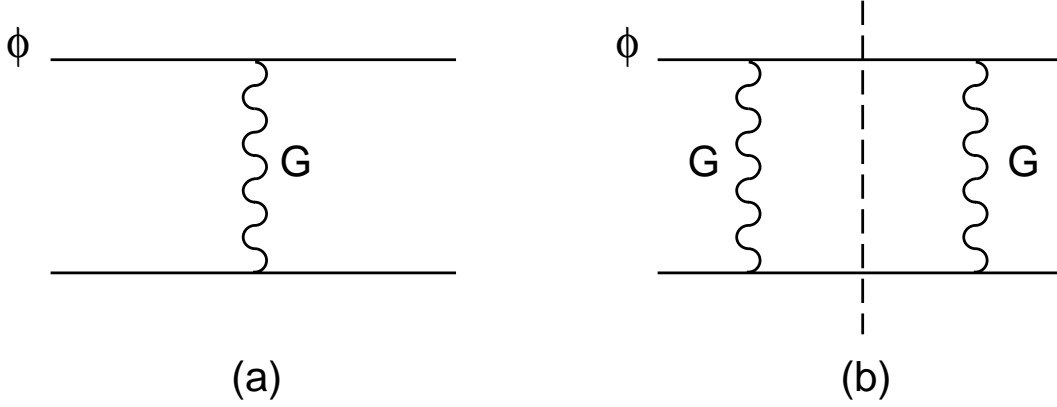


Figure 1: The dominant Feynman diagrams contributing to elastic scattering of Φ particles in the eikonal approximation at tree (a) and one-loop (b) level. Wavy lines represent the exchange of D -dimensional gravitons, and the dashed line represents the cut from the physical-region singularity.

universality of bosons and fermions is not surprising since, as discussed in the introduction, we are performing a semi-classical calculation, and the spin of the Φ particle should not matter.

The tree-level exchange of a D -dimensional graviton in the diagram of fig. 1a gives the scattering amplitude

$$\mathcal{A}_{\text{Born}}(-t) = \frac{s^2}{M_D^{n+2}} \int \frac{d^n q_T}{t - q_T^2} = \pi^{\frac{n}{2}} \Gamma(1 - n/2) \left(\frac{-t}{M_D^2} \right)^{\frac{n}{2}-1} \left(\frac{s}{M_D^2} \right)^2, \quad (11)$$

where q_T is the momentum transfer in the extra dimensions. Although eq. (11) is a tree-level amplitude, it is divergent due to the infinite number of (extra-dimensional) momentum configurations of the exchanged gravitons, allowed by the non-conservation of momenta transverse to the brane. Divergences have been subtracted using dimensional regularization, considering non-integer n , but the regularization prescription is not important since the eikonalization will consistently eliminate any ultraviolet sensitivity. Basically this is because the eikonalization selects in eq. (11) only the partial waves with large angular momentum. These do not depend on the local counter-terms as they are determined by the finite (calculable) non-analytic terms in $-t$, which depend only on infrared physics [3]. These terms are proportional to $(-t)^{(n-2)/2} \ln(-t)$ for even n , and to $\sqrt{-t}(-t)^{(n-3)/2}$ for odd n .

Let us now turn to the one-loop amplitude. The leading term in the limit of small momentum transfer is given by a Feynman diagram with a cut arising from a physical-region singularity in which the intermediate Φ particles are on their mass shells. There is only one such diagram at one loop, and it is drawn in fig. 1b. All other diagrams are subleading. For instance, the one-loop t -channel exchange of two gravitons G coupled via quartic $GG\Phi\Phi$ vertices is suppressed¹ by a power of t/s . Diagrams with one $GG\Phi\Phi$ vertex and two $G\Phi\Phi$ vertices simply vanish (as is evident by working in the de Donder gauge).

The diagram of fig. 1b with on-shell intermediate states can be calculated using the Cutkosky rule. Its imaginary part is $1/2$ times the discontinuity across the cut, which is obtained by replacing the Φ propagators in eq. (10) with $2\pi i\delta(2pq)$. If p_1 and p_2 are the momenta of the incoming particles, we obtain

$$\begin{aligned}\mathcal{A}_{1\text{-loop}}(-q^2) &= \frac{-i}{2} \left(\frac{s^2}{M_D^{n+2}} \right)^2 \int \frac{d^4k}{(2\pi)^4} d^n k_T d^n k'_T \frac{1}{k^2 - k_T^2} \frac{1}{(q - k)^2 - k_T'^2} (2\pi i)^2 \delta(2p_1 k) \delta(2p_2 k) \\ &= \frac{i}{4s} \int \frac{d^2 k_\perp}{(2\pi)^2} \mathcal{A}_{\text{Born}}(k_\perp^2) \mathcal{A}_{\text{Born}}[(q_\perp - k_\perp)^2].\end{aligned}\quad (12)$$

The delta functions from the Cutkosky rule had the effect of reducing the 4-dimensional integral into a 2-dimensional integral over momenta perpendicular to the beam (and along the brane). Notice that, in the eikonal limit, the momentum transfer q is mainly in the perpendicular direction and therefore, we can use the approximation

$$t = q^2 \simeq -q_\perp^2. \quad (13)$$

Equation (12) is merely a convolution of the Born amplitude. It is then convenient to perform a Fourier transform of the amplitudes with respect to the transverse momentum q_\perp . This amounts to trading q_\perp with its conjugate variable b_\perp , the impact parameter. In impact parameter space eq. (12) becomes a simple product. Summing eq. (11) and eq. (12), and transforming back to momentum space we can recast the loop expansion in the form

$$\mathcal{A}_{\text{Born}}(q_\perp^2) + \mathcal{A}_{1\text{-loop}}(q_\perp^2) + \dots = -2is \int d^2 b_\perp e^{iq_\perp b_\perp} \left(i\chi - \frac{1}{2}\chi^2 + \dots \right), \quad (14)$$

¹Actually, in the spirit of the eikonal resummation, this diagram should be compared to the tree-level graviton exchange, but an analogous suppression factor would nevertheless appear.

$$\chi(b_\perp) = \frac{1}{2s} \int \frac{d^2 q_\perp}{(2\pi)^2} e^{-iq_\perp b_\perp} \mathcal{A}_{\text{Born}}(q_\perp^2). \quad (15)$$

The combinatorics of higher-order loop terms is such that one can resum all terms in eq. (14) to obtain

$$\mathcal{A}_{\text{eik}} = -2is \int d^2 b_\perp e^{iq_\perp b_\perp} (e^{i\chi} - 1). \quad (16)$$

We have recovered the known result [8] that the eikonal scattering phase χ , function of the impact parameter plane coordinates b_\perp , is the 2-dimensional Fourier transform of the Born amplitude in the direction perpendicular to the beam.

One crucial feature of the eikonal procedure is that $\chi(b)$ for $b \neq 0$ depends only on the calculable, ultraviolet finite, terms in A_{Born} . The ultraviolet divergent terms correspond to *delta*-function singularities localized at $b = 0$. While these terms are obviously irrelevant for scattering processes where the initial states are prepared in such a way that they have no overlap at $b = 0$, we will also define our full amplitude in eq. (16) by neglecting these terms. We believe this to be a consistent procedure. Indeed, it would not make any sense to include δ -functions in the exponent of eq. (16). From a physical point of view, we expect these singularities to be softened by the fundamental theory of gravity, at some finite, but small, impact parameter $b \sim \lambda_P$ (or, more likely, $b \sim \lambda_S$). So the presence of these terms is just evidence that there should be corrections to our simple eikonal expression coming from the underlying theory of quantum gravity. We will discuss these effects in sect. 2.5. For the moment we limit ourselves to note that these short-distance contributions should plausibly give rise to $\mathcal{O}(\lambda_P^2)$ corrections to the cross section, while, as we will see shortly, the long-distance eikonal amplitude gives a cross section that grows with a power of \sqrt{s} , thus dominating at large energies.

We can now calculate explicitly the eikonal phase χ in eq. (15). One finds (see appendix)

$$\chi = \frac{\pi^{\frac{n}{2}-1} \Gamma(1 - n/2) s}{4M_D^{n+2}} \int_0^\infty dq q^{n-1} J_0(qb) = \left(\frac{b_c}{b} \right)^n, \quad (17)$$

$$b_c \equiv \left[\frac{(4\pi)^{\frac{n}{2}-1} s \Gamma(n/2)}{2M_D^{n+2}} \right]^{1/n}. \quad (18)$$

Here $q \equiv |q_\perp| \simeq \sqrt{-t}$, $b \equiv |b_\perp|$ and J_0 is the zero-th order Bessel function. Notice that by inserting this result for χ in the integral in eq. (16) we obtain an ultraviolet finite result. This is so, even though the contributions to eq. (16) from the individual terms in the expansion of $e^{i\chi} = 1 + i\chi + \dots$ are ultraviolet divergent, corresponding to the fact that each individual Feynman diagram in the ladder expansion is ultraviolet divergent but the complete sum is finite. Moreover, since $\chi \propto b^{-n}$, the integrand in eq. (16) oscillates very rapidly as $b \rightarrow 0$, showing that the ultraviolet region gives but a small contribution to the amplitude.

Replacing eq. (17) into eq. (16), we obtain the final expression for the eikonal amplitude [17]

$$\mathcal{A}_{\text{eik}} = 4\pi s b_c^2 F_n(b_c q), \quad (19)$$

$$F_n(y) = -i \int_0^\infty dx x J_0(xy) (e^{ix^{-n}} - 1), \quad (20)$$

where the integration variable is $x = b/b_c$. The functions F_n , which can be written in terms of Meijer's G-functions, are shown in fig. 2.

At small y , the functions $F_n(y)$ can be expanded as (see appendix)

$$F_2(y) \underset{y \rightarrow 0}{=} -\ln \frac{y}{1.4} + i\frac{\pi}{4} \quad (21)$$

$$F_3(y) \underset{y \rightarrow 0}{=} \frac{i}{2} \Gamma\left(\frac{1}{3}\right) e^{i\frac{\pi}{3}} - y \quad (22)$$

$$F_4(y) \underset{y \rightarrow 0}{=} i\frac{\sqrt{\pi}}{2} e^{i\frac{\pi}{4}} + \frac{y^2}{4} \ln y \quad (23)$$

$$F_n(y) \underset{y \rightarrow 0}{=} \frac{i}{2} \Gamma\left(1 - \frac{2}{n}\right) e^{-i\frac{\pi}{n}} - \frac{i}{16} y^2 \Gamma\left(1 - \frac{4}{n}\right) e^{-i\frac{2\pi}{n}} \quad \text{for } n > 4. \quad (24)$$

These functions develop non-analytic terms in y^2 of the form $y^{n-2} \ln y$ for even n , and y^{n-2} for odd n , which reproduce the non-analytic structure of $\mathcal{A}_{\text{Born}}$ previously mentioned. Notice that $F_n(0)$ is finite for $n > 2$.

For $y \gg 1$ ($q \gg b_c^{-1}$), the stationary-phase approximation applies, yielding

$$F_n(y) \underset{y \gg 1}{=} \frac{-in^{\frac{1}{n+1}} y^{-\frac{n+2}{n+1}}}{\sqrt{n+1}} \exp \left[-i(n+1) \left(\frac{y}{n} \right)^{\frac{n}{n+1}} \right]. \quad (25)$$

The function F_n oscillates around its asymptotic value given in eq. (25), before converging to it at large y , as illustrated in the bottom-right panel of fig. 2.

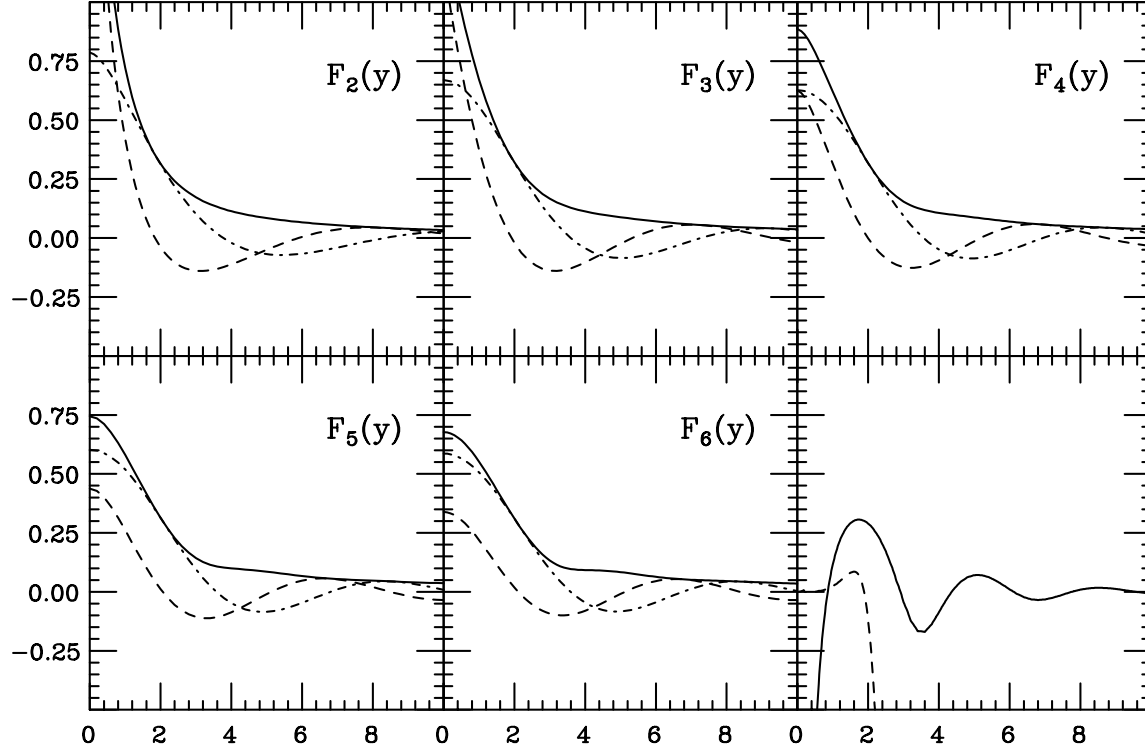


Figure 2: Plots of the function $F_n(y)$ versus y for n between 2 and 6. The dashed line is the real part, the dash-dotted line is the imaginary part, and the solid line is the absolute value of the function. The bottom right panel plots the relative error of $|F_6(y)|$ compared to the asymptotic expressions, see Eqs. (24) and (25), as $y \rightarrow 0$ (dashed line) and $y \rightarrow \infty$ (solid line).

	$n =$	2	3	4	5	6
$A_n =$	$\left[\frac{2^n \pi^{\frac{n-3}{2}} \Gamma(\frac{n+3}{2})}{n+2} \right]^{\frac{2}{n+1}}$	0.83	1.79	3.01	4.42	5.96
$B_n =$	$\left[2^{n-3} \pi^{\frac{n-2}{2}} \Gamma\left(\frac{n}{2}\right) \right]^{\frac{2}{n}}$	0.50	1.35	2.51	3.88	5.41

Table 1: The coefficients A_n and B_n entering eq. (27) and their numerical values for n between 2 and 6.

2.2 Cross Sections

Let us now consider the differential cross section for elastic scattering. From eq. (19) we obtain

$$\frac{d\sigma_{\text{eik}}}{dt} = \pi b_c^4 \left| F_n(b_c \sqrt{-t}) \right|^2. \quad (26)$$

We recall the definitions

$$R_S^2 s = A_n \left(\frac{s}{M_D^2} \right)^{\frac{n+2}{n+1}}, \quad b_c^2 s = B_n \left(\frac{s}{M_D^2} \right)^{\frac{n+2}{n}}, \quad (27)$$

where the coefficients A_n and B_n are given in table 1. In terms of the geometric black-hole cross section $\sigma_{BH} \equiv \pi R_S^2$, eq. (26) can be written as

$$\begin{aligned} \frac{d\sigma_{\text{eik}}}{dt} &= \frac{B_n^{\frac{n}{n+1}}}{A_n} \frac{\sigma_{BH}}{s} (b_c^2 s)^{\frac{n+2}{n+1}} \left| F_n(b_c \sqrt{-t}) \right|^2 \\ &= \frac{B_n^2}{A_n} \frac{\sigma_{BH}}{s} \left(\frac{s}{M_D^2} \right)^{\frac{(n+2)^2}{n(n+1)}} \left| F_n(b_c \sqrt{-t}) \right|^2. \end{aligned} \quad (28)$$

In the limit $q \ll b_c^{-1}$, or equivalently $-t/s \ll B_n^{-1} (M_D^2/s)^{1+2/n}$, the differential cross section becomes (for $n > 2$)

$$\begin{aligned} \frac{d\sigma_{\text{eik}}}{dt} &= \frac{[\Gamma(1 - 2/n)]^2 B_n^{\frac{n}{n+1}}}{4A_n} \frac{\sigma_{BH}}{s} (b_c^2 s)^{\frac{n+2}{n+1}} \\ &= \frac{[\Gamma(1 - 2/n)]^2 B_n^2}{4A_n} \frac{\sigma_{BH}}{s} \left(\frac{s}{M_D^2} \right)^{\frac{(n+2)^2}{n(n+1)}}. \end{aligned} \quad (29)$$

In the opposite limit ($q \gg b_c^{-1}$), we find

$$\frac{d\sigma_{\text{eik}}}{dt} = \frac{(n^2 B_n^{\frac{1}{n+1}})}{(n+1)A_n} \frac{\sigma_{BH}}{s} \left(-\frac{s}{t}\right)^{\frac{n+2}{n+1}}. \quad (30)$$

Notice how the two formulæ valid in the two regimes match since, for $-t \simeq b_c^{-2}$, eq. (30) parametrically agrees with eq. (29). Moreover, extrapolating eq. (30) beyond its range of validity towards small impact parameters (*i.e.* large angle, or $t \rightarrow -s$), we find a result that matches parametrically the black-hole production cross section derived from dimensional analysis.

The integrated elastic cross can be derived directly from eq. (16):

$$\begin{aligned} \sigma_{\text{el}} &= \frac{1}{16\pi^2 s^2} \int d^2 q_{\perp} |\mathcal{A}_{\text{eik}}|^2 \\ &= \int d^2 b_{\perp} \left(1 + e^{-2\text{Im}\chi} - 2e^{-\text{Im}\chi} \cos \text{Re}\chi\right). \end{aligned} \quad (31)$$

The total cross section, inclusive of elastic and inelastic channels, can be derived from the optical theorem

$$\sigma_{\text{tot}} = \frac{\text{Im}\mathcal{A}_{\text{eik}}(0)}{s} = 2 \int d^2 b_{\perp} \left(1 - e^{-\text{Im}\chi} \cos \text{Re}\chi\right). \quad (32)$$

In the absence of absorptive parts ($\text{Im}\chi = 0$) eq. (31) and eq. (32) coincide. Black-hole production may be modelled by a large absorptive part ($\text{Im}\chi \gg 1$) at impact parameters smaller than R_S .

2.3 Physical Interpretation

Before proceeding to the phenomenological analysis, we remark on the physical meaning of the expression of the eikonal amplitude given by eq. (16) and eq. (17). We can first consider a non-relativistic analogue of the problem under investigation [23] by studying the scattering of a particle with mass m , velocity v , and impact parameter b by a radial “gravitational” potential

$$V(r) = \frac{G_D m M}{r^{n+1}}. \quad (33)$$

Here m and M are the non-relativistic analogues of $\sqrt{s}/(2c^2)$, v is the analogue of c , and n corresponds to the number of extra dimensions.

When b is not too small, the quantum-mechanical scattering phase of the wave associated with angular momentum $\ell\hbar = mvb$ is

$$\delta_b = -\frac{1}{v\hbar} \int_b^\infty dr V(r). \quad (34)$$

The intergral in eq. (34) converges only for $n > 0$, leading to $\delta_b = -(b_c/b)^n$, where $b_c \simeq [G_D m M / (\hbar v)]^{1/n}$ exactly corresponds to the definition in eq. (18). Therefore, the forward amplitude (which is proportional to $\int db b \delta_b$) is finite only for $n > 2$. For $n = 0$ one finds the Coulomb singularity, and for $n = 2$ a logarithmic divergence. This is in agreement with eq. (24) and with the relativistic results presented in sect. 2.1.

A classical description of the process is valid if the quantum-mechanical uncertainties in the impact parameter b and in the scattering angle θ are small with respect to their classical values. Using the Heisenberg principle, the quantum uncertainties are estimated to be

$$\Delta\theta \sim \frac{\Delta q}{mv} \sim \frac{\hbar}{mv\Delta b}, \quad (35)$$

where q is the momentum in the direction orthogonal to the initial velocity \vec{v} . The classical scattering angle is equal to the force (dV/dr) at the minimum distance ($r = b$), times the collision time (b/v), divided by the momentum (mv),

$$\theta \sim \frac{b}{mv^2} \frac{dV(b)}{db}. \quad (36)$$

The condition for the validity of the classical approximation ($\Delta\theta \ll \theta$, $\Delta b \ll b$) implies $|dV(b)/db| > \hbar v/b^2$. For a Coulomb-like potential $V(r) = \alpha/r$, this condition is satisfied in the non-perturbative region $\alpha > \hbar v$. In our case, it implies (for $n > 0$) $b < b_c$, with $b_c \sim [G_D m M / (v\hbar)]^{1/n}$. The length scale b_c is a quantum scale ($b_c \rightarrow \infty$ as $\hbar \rightarrow 0$) characteristic of the extra-dimensional scattering (it is undefined at $n = 0$). Therefore, at $b > b_c$, quantum mechanical effects cannot be neglected.

In the classical process (for $n > -1$), a projectile with an arbitrarily large impact parameter b is deflected by a non-vanishing (although very small) angle, and therefore the cross

section diverges at $q = 0$ ($b \rightarrow \infty$). In our case, for $b > b_c$, quantum mechanics sets in, and the quantum fluctuations of the scattering angle become larger than its classical value, rendering ill-defined the notion of a trajectory. This is why the quantum scattering amplitude can remain finite at $q \rightarrow 0$.

It is also interesting to compare the result of eq. (19) with the fully D -dimensional case, in which both gravity and the colliding particles propagate in the extra dimensions [10]. In this case eq. (16) becomes

$$\mathcal{A}_{\text{eik}} = -2is \int d^{2+n} b_{\perp} e^{iq_{\perp} b_{\perp}} \left[e^{i(b_c/b_{\perp})^n} - 1 \right]. \quad (37)$$

For $q = 0$, the integral is infrared dominated by large values of b and it is quadratically divergent (for any n). Therefore we find $\mathcal{A}_{\text{eik}}(q \rightarrow 0) \sim b_c^n/q^2$, and we encounter the Coulomb singularity characteristic of long-range forces. On the other hand, in the case of particles living on the 3-brane, we have found (for $n > 2$) that the forward scattering amplitude is finite and that, although the force does not have a finite range, the integral in eq. (16) at $q = 0$ is dominated by distances of order b_c . Indeed, by working with localized particles we lose momentum conservation in the transverse direction, and moreover the Born amplitude becomes dominated by contact terms of ultraviolet origin. The fact that eq. (16) is not infrared dominated even for $q \rightarrow 0$ is a remnant of this property of the Born amplitude.

Let us now come back to the relativistic elastic scattering under consideration. As we have seen in sect. 2.1, there exist two different kinematic regions in which the eikonal amplitude has distinct behavior.

Region (i): $\sqrt{s} \gg q \gg b_c^{-1}$.

This is the region in which the integral in eq. (20) is dominated by the stationary-phase value of the impact parameter $b = b_s$, where

$$b_s \equiv b_c \left(\frac{n}{qb_c} \right)^{\frac{1}{n+1}} = \frac{(nB_n^{n/2})^{\frac{1}{n+1}}}{\sqrt{s}} \left(-\frac{t}{s} \right)^{-\frac{1}{2(n+1)}} \left(\frac{s}{M_D^2} \right)^{\frac{n+2}{2(n+1)}}. \quad (38)$$

In this region $b < b_c$, and therefore the eikonal phase $\chi = (b_c/b)^n$ is large (in units of \hbar): we are in the classical domain. Indeed, the classical scattering angle is given by the derivative

of the scattering phase with respect to the angular momentum $L = \sqrt{s}b/2$,

$$\theta_{\text{cl}} = -\frac{\partial\chi}{\partial L} = \frac{2n\Gamma(n/2)}{\pi^{n/2}} \frac{G_D\sqrt{s}}{b^{n+1}}. \quad (39)$$

In the limit $n \rightarrow 0$, we recover the Einstein angle $\theta_{\text{cl}} = 4G_D\sqrt{s}/b$ while, for $n > 0$, eq. (39) gives its higher-dimensional generalization². Notice that the relation between scattering angle and impact parameter in eq. (39) is equivalent to $b = b_s$.

Region (ii): $q \ll b_c^{-1}$.

In this region the integral in eq. (20) is dominated by b of the order of (or slightly smaller than) b_c . This means that the eikonal phase $\chi = (b_c/b)^n$ is of order one (in units of \hbar) and the quantum nature of the scattering particles is important (although the exchanged graviton is treated as a classical field, and so quantum gravity effects are negligible), as we could have expected from the discussion of the non-relativistic analogue presented above. There is no one-to-one relation between impact parameter and scattering angle in region (ii), since the classical concept of a trajectory is not applicable. Moreover, notice that the relevant χ never becomes much smaller than 1, and therefore we never enter the perturbative regime in which a loop expansion for the amplitude applies. Even though the interaction vanishes at $b \rightarrow \infty$ (where $\chi \rightarrow 0$), we never reach the Born limit. Even for $q = 0$, the scattering is dominated by $b = b_c$ and not by $b = \infty$, as in the Coulomb case. As explained after eq. (37), this result simply follows from the different dimensionalities of the spaces relevant for scattering particles (living on a 3-brane) and exchanged graviton (propagating in the bulk), and it does not hold in the case of scattering of bulk particles.

2.4 Corrections to the Eikonal Approximation

The conditions required by our approximations are expressed in eq. (8). In order to assess the theoretical uncertainty inherent to our calculation, in this section we estimate the size of the effects that we have neglected. We first discuss classical effects, for which general

²The Einstein angle defines the deflection of a photon by the static gravitational field of a mass- M particle at rest: $\theta_E = 4G_N M/b$. It is easy to see that by boosting θ_E to the center-of-mass frame, in the limit $\sqrt{s} \gg M$, we obtain our expression of θ_{cl} .

relativity suffices. We also include the quantum-mechanical effects of region *(ii)*, but we leave quantum-gravity contributions for the next section. The neglected classical terms come from the approximations of small angle ($-t/s \ll 1$) and of weak gravitational field ($R_S/b \ll 1$). Associated with the subleading classical effects there is also the emission of gravitational radiation, leading to missing energy signals at high-energy colliders.

Let us estimate these effects. Notice that in the classical region *(i)* where $\sqrt{s} \gg q \gg b_c^{-1}$, the two requirements coincide since $b = b_s$, see eq. (38). Here, scattering can be described in terms of classical trajectories. The equation $b = b_s$ represents a relation between transferred momentum and impact parameter

$$-\frac{t}{s} \sim \frac{G_D^2 s}{b^{2n+2}} \sim \left(\frac{R_S}{b}\right)^{2n+2}, \quad (40)$$

where we have neglected factors of order unity. This result represents an approximation [13] in which one considers only a linear superposition of the gravitational shockwave fields generated by the two colliding particles [14], thereby neglecting non-linear effects of their mutual interactions. In this computation, each field represents an exact solution to Einstein's equations in the absence of the other field. Inclusion of the non-linear effects will induce $\mathcal{O}(G_D^p)$ corrections to eq. (40), where p is an unknown power. By dimensional analysis the relative size of these corrections must be $G_D^p s^{p/2}/b^{p(n+1)} \sim (R_S/b)^{p(n+1)}$. Moreover since we expect that the evaluation of these effects is perfectly perturbative, analyticity in s should hold, and therefore only even integers of the exponent p will appear. We conclude that eq. (40) will be corrected by a factor of the form

$$1 + \mathcal{O}\left(\frac{G_D^2 s}{b^{2n+2}}\right) = 1 + \mathcal{O}\left(\frac{t}{s}\right). \quad (41)$$

This will induce a correction of the same size to the cross section, in the classical region *(i)*. Notice that eq. (41) corresponds to a $\mathcal{O}(\theta^3)$ correction term to the relation between scattering angle and impact parameter, eq. (39). In the scattering by a static potential we would get corrections already at $\mathcal{O}(\theta^2)$. Our different result follows from the relativistic nature of the process.

In region (ii) where $q \ll b_c^{-1}$, the leading correction to the cross section will then have the form

$$\frac{d\sigma}{dt} = \frac{d\sigma_{\text{eik}}}{dt} \left[1 + \frac{t}{s} Z(tb_c^2) \right], \quad (42)$$

where Z is expected to be a constant of order unity in the classical region $tb_c^2 \gg 1$. In the region $tb_c^2 \ll 1$, the quantum nature of the scattering particles becomes relevant, and Z will have non-trivial behavior. However, admitting only finite corrections at $t \rightarrow 0$ implies that the size of the relative correction to $d\sigma/dt$ is at most $1/sb_c^2 \sim (R_S/b_c)^{2n+2}$.

In summary, we have inferred that the leading classical gravity corrections to the eikonal amplitude are

$$\mathcal{O}\left(-\frac{t}{s}\right) + \mathcal{O}\left[\left(\frac{M_D^2}{s}\right)^{1+\frac{2}{n}}\right], \quad (43)$$

and therefore suppressed and under control for the conditions we are applying, as expressed by eq. (8).

The discussion outlined above is consistent with the analysis of ref. [10] where classical corrections to the eikonal are identified by resumming an improved ladder series including a class of two-loop graphs, the so-called H-diagrams. After improving the Born term by the H-diagram, the eikonal phase is modified to

$$\chi \rightarrow \left(\frac{b_c}{b}\right)^n \left[1 + \mathcal{O}\left(\frac{R_S}{b}\right)^{2n+2} \right]. \quad (44)$$

It is easy to check that altering eq. (16) according to the above equation produces corrections to the leading amplitude consistent with eq. (43). Notice that the corrections to the eikonal become large for impact parameters comparable to the Schwarzschild radius, for which the production of black holes presumably sets in³.

Gravitational radiation is associated with subleading classical effects. Emission of gravitons is signaled by the presence of an imaginary part in the H-diagram contribution to the

³The hypothesis that classical physics determines the black-hole production cross section has been criticised in ref. [21]. However, we believe that the appearance of corrections of the form shown in eq. (44) is a further indication that non-trivial classical dynamics emerges at $b \simeq R_S$.

eikonal phase [10]

$$\begin{aligned}\text{Im}(\chi_H) &\sim \left(\frac{b_r}{b}\right)^{3n+2}, \\ b_r &\equiv \left(b_c^n R_s^{2n+2}\right)^{\frac{1}{3n+2}} \sim \left(G_D^3 s^2\right)^{\frac{1}{n+2}}.\end{aligned}\tag{45}$$

This absorptive term corresponds to a depletion of purely elastic scattering due to the emission of gravitational radiation. When $b \ll b_r$ the probability of elastic scattering becomes exponentially small. The calculation of ref. [10] shows that the emitted radiation has typical transverse momentum $\sim 1/b$. However the longitudinal momentum is distributed up to values of order \sqrt{s} . Therefore we expect that for $b < b_r$ a significant fraction of the energy is radiated in the form of forward gravitational radiation. Notice that $b < b_r$ is typically outside our chosen kinematical regime, so that we expect only a fraction $\sim (b_r/b)^{3n+2} \ll 1$ of initial energy to be lost to invisible gravitational radiation. In the semiclassical region, we find $(b_r/b)^{3n+2} \simeq (-t/s)^{n/(n+1)}(\sqrt{-t}/M_D)^{(n+2)/(n+1)}$, and therefore gravitational radiation for small-angle scatterings is not large.

One may worry that important emission of radiation, already at $b \gg R_s$, may drastically reduce the naive geometric estimate of the black-hole production cross-section. Indeed if one simply interpreted eq. (45), *à la* Block-Nordsiek, as the number N of emitted gravitons, one would conclude that hard bremsstrahlung depletes all the energy, as soon as b is smaller than b_r . However this naive interpretation is manifestly inconsistent as the total emitted energy would quickly exceed \sqrt{s} . Indeed it is likely that the exponentiation of the H-diagram imaginary part is inconsistent for hard radiation. On the other hand for soft radiation with $E \sim 1/b$, the Block-Nordsiek interpretation is likely to be reasonable. Thus if the number of soft gravitons is $N_{\text{soft}} \sim (b_r/b)^{3n+2}$ then the total energy lost to soft radiation at large angle is

$$E_{\text{rad}} \sim \frac{N_{\text{soft}}}{b} \sim \sqrt{s} \left(\frac{R_s}{b}\right)^{3n+3},\tag{46}$$

which becomes important only for $b \sim R_s$.

2.5 Quantum-Gravity Effects

On general grounds we expect that quantum-gravity contributions to the eikonal phase must be of the form $\delta\chi/\chi \sim (\lambda_P/b)^k$, with $k > 0$ and λ_P given in eq. (2). If we work in the true transplanckian region ($\sqrt{s} \gg M_D$), these effects are subleading⁴ since, as we have discussed in sect. 1, the classical scale R_S is much larger than the quantum scale λ_P .

However, as it will be clear in the following, collisions at the LHC can only barely satisfy the transplanckianity condition. Therefore, quantum-gravity corrections are potentially large, and they are likely to be the limiting factor of our approximations. This happens because, although quantum-gravity effects are characterized by a length scale λ_P smaller than the Schwarzschild radius R_S , classical corrections appear with a large exponent, see eqs. (41) and (43), remnant of the geometric nature of the interaction, while this is not expected to be the case for the quantum-gravity corrections $\mathcal{O}(\lambda_P/b)^k$.

However in order to be able to say more we need a quantum-gravity model or at least a framework. String theory is the only possibility at hand, and the transplanckian regime has been discussed in this context by several authors, see *e.g.* refs. [10, 11, 24]. Indeed, we will show that string corrections appear to be large for energies relevant to LHC experiments.

In ref. [10] string corrections to eikonalized graviton scattering for type II superstrings were studied. Since we do not stick to a particular string realization of our brane-world scenario, we will limit ourselves to a qualitative discussion. Following ref. [25] we may imagine a realization of the brane-world in type I, where $m = 6 - n$ spatial dimensions out of the 10 space-time dimensions are compactified on a torus T^m with radius $r_m = \sqrt{\alpha'} = 1/M_S$, and M_S is the string scale. Of the remaining dimensions, n have a “large” compactification radius and 3 are the usual non-compact ones. The brane-world is realized by a $(3 + m)$ -

⁴It is interesting to compare the case of gravity with the case of vector-boson exchange which has been mentioned in sect. 1. For a vector, the eikonal phase is $\chi_V \propto e^2/b^n = 1/(M_e b)^n$ (we take $\hbar = c = 1$). Notice that, as opposed to gravity, there is no factor of s enhancement [9]. It is easy to realize that quantum corrections will also go like a power of e^2/b^n . This is for instance the case for vacuum-polarization improvement of the vector propagator. Therefore, there is no impact parameter choice for which both $\chi_V \gg 1$ and quantum corrections are small, where the eikonal approximation can be useful.

dimensional D-brane, in which m dimensions span the small manifold T^m . In terms of M_S and of the string coupling g_S , the $4+n$ dimensional Planck scale M_D and the gauge coupling g on the brane are given by

$$M_D^{2+n} = \frac{e^{-2\phi}}{\pi} M_S^{2+n}, \quad \frac{1}{g^2} = \frac{e^{-\phi}}{2\pi}, \quad g_S = e^\phi, \quad (47)$$

where ϕ is the dilaton vacuum expectation value. Of course these relations will receive corrections of order unity in realistic models with broken supersymmetry and should be viewed, here and in the following, only as indicative estimates. Equations (47) imply

$$\left(\frac{M_S}{M_D}\right)^{2+n} = \frac{g^4}{4\pi}. \quad (48)$$

If we identify g with the gauge couplings of the SM, say for instance $g = g_{\text{weak}}$, we conclude that there should be a mild hierarchy between M_D and M_S . For instance, we find M_D/M_S equals 1.7 and 2.8 for $n = 6$ and $n = 2$, respectively. *A priori* one could also conceive string models where M_D and M_S coincide, with a self-dual dilaton vacuum expectation value $\phi \sim 0$, corresponding to a strongly coupled string. In this case the weakness of the SM gauge couplings would have to be explained by some additional mechanism.

As we will discuss in sect. 3.1, in order to observe transplanckian scatterings at the LHC, we have to consider values of M_D smaller than a few TeV. The existence of string theory at such a low scale is already limited by precision electroweak data and by the non-observation of new contact interactions at LEP. Exchanges of gravitons and massive string states give rise to effective operators involving SM fields. The leading effects come from 4-fermion operators of dimension 6 which, if present at tree level, give an approximate bound $M_S > 3$ TeV [26]. This bound is in conflict with the working assumptions necessary to have observable transplanckian signals at the LHC, and therefore we have to assume a mild suppression of the dimension-6 operators. This assumption is probably not unreasonable, as there exist examples [6, 26] where these effects vanish at tree level. In this respect the presence of supersymmetry at some stage in the construction may help suppress these contributions. Loop effects are within current experimental bounds even for M_D of order a few TeV, if the underlying quantum-gravity theory does not become strongly-interacting or,

in a more operative sense, if the divergent loops are cut off at a scale slightly smaller than M_D [27]. This allows for the weakly-interacting string scenario in which there is a small hierarchy between M_S and M_D , but it essentially rules out the case of strongly-coupled strings with M_S of a few TeV, where we would need the rather strong, and implausible, assumption that dimension-6 operators are suppressed to all orders in perturbation theory.

With these limitations in mind we now consider string corrections [10]. The basic result is that the eikonal elastic field-theory amplitude gets promoted to a unitary matrix acting non-trivially over a subspace of the string Fock space

$$\begin{aligned} \exp \left[i \left(\frac{b_c}{b} \right)^n \right] &\rightarrow \exp \left[i \left(\frac{b_c}{b} \right)^n \right] K, \\ K &= \exp \left[i \left(\frac{b_D}{b} \right)^{n+2} \hat{H} \right], \quad b_D^{n+2} \equiv \alpha' b_c^n. \end{aligned} \quad (49)$$

Here \hat{H} is a hermitian operator involving the creation and annihilation operators for the string oscillator modes. The above equation shows that, for $b < b_D$, a diffractive production of excited string modes takes place without any suppression. Basically what happens is that the two colliding partons are excited into string modes through multiple soft graviton exchange.

The average mass of the string modes is roughly given by $M_S(b_D/b)^{n+2}$. This is smaller than the available energy \sqrt{s} as long as $(R_S/b)^{n+1}(\sqrt{\alpha'}/b) < 1$. This condition is clearly satisfied within our chosen kinematical regime, and therefore the produced particles are relativistic. The opening of an (exponentially) large number of new channels drastically depletes the elastic one. For instance in the example discussed in ref. [10], where gravitons are scattered in type II superstring, the elastic amplitude correction factor becomes

$$\langle K \rangle = \Gamma^{2n+2}(1 - i\Delta)\Gamma^2[1 - i(n+1)\Delta], \quad (50)$$

where $\Delta = (n/2)(b_D/b)^{n+2}$ and where by $\langle K \rangle$ we indicate the expectation value of the operator K on the initial state.

For $b \gg b_D$, the correction factor in eq. (50) becomes

$$\langle K \rangle \simeq 1 + i 2 \gamma n(n+1) \left(\frac{b_D}{b} \right)^{n+2}, \quad (51)$$

where $\gamma = 0.577$ is the Euler number. Therefore, the effects of string excitations set in much before the string scale. Already at $b \sim b_c$, the terms modifying the gravitational eikonal phase implied by eq. (51) are as large as $n(n+1)(M_D^2/M_S^2)(M_D^2/s)^{2/n}$. As we have previously anticipated, these effects can be much more sizable than the classical corrections in eq. (43), even if the string length is smaller than the classical Schwarzschild radius.

For $b \ll b_D$, we find

$$|K| \simeq (n+1)(\pi n)^{n+2} \left(\frac{b_D}{b} \right)^{(n+2)^2} \exp \left[-\pi n(n+1) \left(\frac{b_D}{b} \right)^{(n+2)} \right], \quad (52)$$

showing that the absolute value of the correction factor decreases exponentially at $b < b_D$, because of the appearance of the string excitations.

This string effect is fairly general and we expect it in realistic models not to differ too much from eq. (50). However the sharp drop in the elastic cross section can be compensated by looking at the inclusive diffractive cross section. Since $b_D < b_c$ we can use the saddle point approximation to evaluate the amplitude in transverse momentum space

$$\mathcal{A}(q) = \mathcal{A}_{\text{eik}}(q) \exp \left[i \left(\frac{b_D}{b_s(q)} \right)^{n+2} \hat{H} \right], \quad (53)$$

where \mathcal{A}_{eik} is the eikonal amplitude in the stationary phase regime. Due to unitarity of the second factor, the total cross-section obtained by summing on the diffractive channels is just the same as in the absence of strings, *i.e.* there is no exponential suppression. Notice that this inclusive cross section is consistently defined in the limit in which the string modes are relativistic: at a fixed q all modes come out at essentially the same angle θ . The question of how well one can measure experimentally the inclusive cross section depends very much on the model, and in particular on the decay properties of the produced string modes. These states are excited by gravitons, so that they have the same color and electric charge of the

incoming partons. If they are stable, the final state of the collision is given by two (massive) jet events. If they are unstable and their dominant decay mode involves bulk states, like the graviton, then the presence of missing energy would make it impossible to deduce the original center-of-mass energy and to make sure that only events at a given center-of-mass energy are selected. On the other hand if they dominantly decay on the brane this reconstruction might be possible. Notice that the coupling to bulk modes (closed strings) and to brane modes (open strings) are proportional to g_S^2 and g_S , respectively. Therefore the decay to brane modes, when possible, dominates over bulk decays in weakly-coupled string models.

We also want to comment on the string effects arising in the regime $M_D < \sqrt{s} < M_S/g_S^2$ [22]. In this regime, although the energy is transplanckian, $\lambda_S > R_S$ holds. Then the large angle, small impact parameter effects are dominated by string physics instead of classical gravitational effects. In this regime one should use the string version of the eikonal phase [10]. The main effect is that $\text{Im}\chi \sim g_S^2 s \alpha' \exp(-b^2/2\alpha' \ln s \alpha')$, corresponding to inelastic production of very excited strings (string balls) dominating the scattering for $b \leq \lambda_S$. The corresponding cross section is $\sim \alpha'$ for $M_S/g_S < \sqrt{s} < M_S/g_S^2$. At $\sqrt{s} \sim M_S/g_S^2$, we have that $\alpha' \sim R_S^2$, consistent with the string balls becoming indistinguishable from ordinary black holes [22]. The onset of inelastic string production marks the end of the validity of our description, since any reminiscence of classical gravitational dynamics is lost.

Notice that in the context of strings there exists another approach to calculate fixed-angle scattering in the regime $\sqrt{s} \gg M_S$ [24]. This different approach leads to an elastic amplitude that vanishes at small fixed angle like $\exp(-\theta\sqrt{\alpha' s})$ [28]. Recently this approach was applied [29] to the TeV string scenario. The conclusions of ref. [24] seem to disagree with those of ref. [10], based on the string eikonal. The elastic amplitude in ref. [10] has a different exponential suppression than that in refs. [24, 28], and is due to gravitational radiation and diffractive string production. Anyway, the discussion of ref. [10] shows that, even if the elastic channel is suppressed, the total cross section at finite angle is large and grows with \sqrt{s} . Notice also that if \sqrt{s} is large enough the average mass of the diffractive states eventually exceeds both M_S and M_D , so it is possible that the diffractive channel becomes at extremely high energies the production of a pair of small black holes.

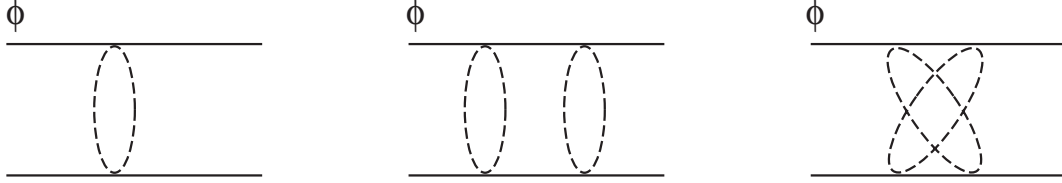


Figure 3: Ladder and cross-ladder Feynman diagrams contributing to elastic scattering of Φ particles. The dashed lines represent the exchange of brane excitations.

Next, we would like to comment on the possible effects of the modes corresponding to the brane motion, the branons [30]. The first comment is that these modes do not necessarily exist. If the SM fields are localized at some fixed point, as in orbifold constructions, then it is consistent to assume that the corresponding “brane” is not a dynamical object, and could also have vanishing tension. So when the SM lives at a fixed point there is no effect (apart from a “trivial” reduction of the phase space of bulk gravitons).

Two types of effects can be associated with brane dynamics. First, the presence of a brane tension $\tau = \mu^4$ gives rise to a gravitational field, which at a transverse distance y from the brane vanishes like $(R_\tau/y)^{n-2}$, where the gravitational radius R_τ is [31]

$$R_\tau^{n-2} = \frac{\Gamma(n/2)2^{n+1}\pi^{\frac{n}{2}}}{\sqrt{(n-1)(n+2)}} \frac{\tau}{M_D^{2+n}}. \quad (54)$$

The wave function of a bulk graviton with transverse momentum k_T is expected to receive a correction of order $(R_\tau k_T)^{n-2}$ from the presence of this background. For a given impact parameter b , the tree-level scattering amplitude is precisely saturated by the exchange of graviton KK modes with mass $\sim 1/b$. Therefore we expect the background metric to correct the eikonal phase by a relative amount $\sim (R_\tau/b)^{n-2}$. For $n > 2$, at large enough impact parameter we can neglect the brane radius as much as we can neglect the Schwarzschild radius R_S . This gravitational brane effect becomes less important as the tension is decreased.

The second class of effects is associated with the exchange of branons. Branon exchange becomes more important the smaller the tension. Notice first of all that at the classical level branons are not excited by the gravitational shockwave of a fast moving particle, *i.e.* the induced metric on the brane remains of the Aichelburg-Sexl kind. At the quantum level,

branons can be exchanged in pairs between the colliding particles. The exchange of a pair of branons is very much equivalent to the exchange of a “composite” graviton. In order to get an estimate of the size of the effect, we may generalize the graviton eikonal including the ladder and cross-ladder diagrams with two-branon blobs (see fig. 3). The eikonal phase gets modified into

$$\chi(b) = \left(\frac{b_c}{b}\right)^n + \frac{n}{120\pi^3} \frac{s}{\tau^2 b^6}. \quad (55)$$

In the case of $n = 6$ the effect is equivalent to a renormalization of G_N , but in all other cases it can distort our result from pure graviton exchange.

Including both effects from brane excitations, we can write the relative correction to the elastic amplitude (in the semiclassical region) as

$$\frac{\delta\mathcal{A}}{\mathcal{A}} = \left(\frac{\mu}{M_D}\right)^4 \left(\frac{M_D\sqrt{-t}}{s}\right)^{\frac{n-2}{n+1}} + \left(\frac{M_D}{\mu}\right)^8 \left(\frac{M_D\sqrt{-t}}{s}\right)^{\frac{6-n}{n+1}}, \quad (56)$$

where we have dropped all numerical factors. This equation shows that for the interesting case $2 < n \leq 6$ and for the natural choice $\mu \sim M_D$, both branon effects are small in the region of small angle and large s . Notice that for a 3-dimensional D-brane arising by wrapping a $(9-n)$ -brane over the $6-n$ dimensions of radius $\sqrt{\alpha'}$ along the lines of the example above, the tension is given by

$$\tau = \frac{e^{-\phi}}{(2\pi)^{\frac{n}{2}} \alpha'^2}. \quad (57)$$

Then at weak coupling we have $R_\tau < \sqrt{\alpha'}$ and the effects of the first class are very small. Effects of the second class are also small as long as $b > \sqrt{\alpha'}$ and $n < 6$. For $n = 6$, the contribution from branon exchange leads to the peculiar result $\chi_{\text{branon}} = \chi_{\text{grav}}/5$, see eq. (55)⁵.

To summarize, quantum-gravity corrections are potentially very sizable because, although they involve smaller length scales, they do not appear with large exponents, as in the case of the semiclassical corrections. Of course, they cannot be computed in the absence of a complete quantum-gravity theory. We have estimated their effects in the context of string

⁵We thank A. Strumia for stressing this result of the physics of D-branes.

theory, borrowing the results of ref. [10] (which are however strictly valid only for graviton-graviton scattering). For $b < b_D$, a diffractive production of string states occurs, depleting the elastic scattering cross section, although it may still be possible to recover the gravitational scattering properties by studying inclusive cross sections. This gravitational excitation of string modes looks like a very promising way to investigate, in a rather clean channel, string effects at high-energy colliders. As the impact parameter is further decreased and becomes of the order of $\lambda_S = \sqrt{\alpha'}$, we are entering the regime of head-on collisions between string modes, with inelastic production of Regge excitations eventually leading to multi-string states [22].

In the following, we will focus on gravitational transplanckian collisions, neglecting quantum-gravity effects. One should keep in mind that such (at the moment incalculable) effects may give significant modifications to the signal discussed below. Although potentially disrupting to the predictivity of the elastic channel, these new-physics effects are of course very interesting from the experimental point of view.

3 Phenomenology in the Transplanckian Regime

3.1 Signals at the LHC

At the LHC, the observable of interest is jet-jet production at small angle (close to beam) with large center-of-mass collision energy. The amplitudes derived in previous sections are applicable for the scattering of any two partons. The total jet-jet cross-section is then obtained by summing over all possible permutations of initial state quarks and gluons, using the appropriate parton distribution weights and enforcing kinematic cuts applicable for the eikonal approximation.

Defining \hat{s} and \hat{t} as Mandelstam variables of the parton-parton collision, we are interested in events that have $\sqrt{\hat{s}}/M_D \gg 1$ and $-\hat{t}/\hat{s} \ll 1$. We can extract $\sqrt{\hat{s}}$ from the jet-jet invariant mass $M_{jj} = \sqrt{\hat{s}}$, and \hat{t} from the rapidity separation of the two jets $-\hat{t}/\hat{s} = 1/(1 + e^{\Delta\eta})$, where $\Delta\eta \equiv \eta_1 - \eta_2$. The variable $\Delta\eta$ is especially useful since it is invariant under boosts along the beam direction, and it is simply related to the $\hat{\theta}$ scattering angle in the center-of-mass

frame:

$$\Delta\eta = \ln \left[\frac{1 + \cos \hat{\theta}}{1 - \cos \hat{\theta}} \right]. \quad (58)$$

Therefore, the kinematical region of interest is defined by the equivalent statements

$$\Delta\eta \rightarrow \infty \quad \leftrightarrow \quad \hat{\theta} \rightarrow 0 \quad \leftrightarrow \quad \frac{-\hat{t}}{\hat{s}} \rightarrow 0. \quad (59)$$

In computing the cross-sections we use the CTEQ5 [32] parton-distribution functions. We have also compared results with GRV [33] and find little difference. We evaluate the parton-distribution functions at the scale $Q^2 = b_s^{-2}$, see eq. (38), if $q > b_c^{-1}$ and $Q^2 = q^2$ otherwise ($q^2 \equiv -\hat{t}$) [17].

We require that both jets have $|\eta| < 5$ and $p_T > 100 \text{ GeV}$ from conservative detector requirements. The SM di-jet cross section is computed using Pythia [34], ignoring higher-order QCD corrections, and the gravitational signal is calculated using our own VEGAS Monte Carlo integrater. For simplicity we are defining the background as the jet-jet cross-section from QCD with gravity couplings turned off, and the signal as the jet-jet cross-section from the eikonal gravity computation with QCD turned off. In reality, SM and gravity contributions would be simultaneously present. Nevertheless, there is no interference between the leading QCD contribution in the limit $t/s \rightarrow 0$ and the gravitational contribution, since graviton couplings are diagonal in color indices. However, terms $\mathcal{O}(\alpha_W)$ are generated by the interference between gravitational and Z/γ contributions. At order $\mathcal{O}(\alpha_s^2)$, the di-jet cross section receives contributions from the square of the amplitude obtained by exchanging 1 gluon and any number of gravitons (resummed in the eikonal approximation) and from the interference between the gravitational amplitude and resummed diagrams with exchange of 2 colored particles and any number of gravitons. In the small regions of parameter space where the QCD and gravity contributions are comparable, these terms, which will not be computed in this paper, should be taken into account. We will not make any detailed claims about that region here.

Although we are working in the transplanckian regime, we are considering processes with low virtuality ($Q^2 \sim 1/b^2 \ll M_D$) and, as long as no new physics appear at momenta smaller

than Q , the SM dynamics give a reliable estimate of the background. In the context of string theory, the QCD background has to be interpreted as the leading contribution from exchange of open strings, in the limit in which the transfer momentum is smaller than the mass of the Regge excitations.

The jet-jet process is best described by the two kinematic variables M_{jj} and $\Delta\eta$. Although experimental searches for new physics in the jet-jet observable should investigate the full range of these two kinematic variables, our goal is to study the region in which the eikonal computation is valid, where we can make reliable theoretical predictions. This leads us to the region of large $\Delta\eta$ and large M_{jj} .

Let us begin by studying the parton differential cross section signal distribution as a function of the rapidity separation $\Delta\eta$ for a fixed $\sqrt{\hat{s}} = M_{jj}$,

$$\frac{d\hat{\sigma}}{d\Delta\eta} = \frac{\pi b_c^4 \hat{s} e^{\Delta\eta}}{(1 + e^{\Delta\eta})^2} |F_n(y)|^2, \quad (60)$$

where $y = b_c \sqrt{\hat{s}} / \sqrt{1 + e^{\Delta\eta}}$. This distribution has a series of peaks whose maxima and minima are determined by the values of $\Delta\eta$ that satisfy the equation

$$1 - e^{-\Delta\eta} = - \frac{y}{|F_n(y)|} \left. \frac{d|F_n(y)|}{dy} \right|_{y=\frac{b_c \sqrt{\hat{s}}}{\sqrt{1+e^{\Delta\eta}}}}. \quad (61)$$

These peaks arise from the oscillations of the function $|F_n|$ around its asymptotic value given in eq. (25), and characterize the transition region between the “classical” (small $\Delta\eta$) and “quantum” (large $\Delta\eta$) regimes discussed in sect. 2. Therefore, we cannot solve eq. (61) using the asymptotic expressions given in eq. (24) or eq. (25). Approximate solutions of eq. (61) can be found if the peaks are located at sufficiently large values of $\Delta\eta$, since in this case we can neglect $e^{-\Delta\eta}$ with respect to 1 in the left-hand side of eq. (61). Then, eq. (61) becomes a function only of the variable y . For our consideration, this approximation is adequate for determining at least the first peak. We find that the first peak of the $\Delta\eta$ distribution, for a fixed value of the two-jet invariant mass M_{jj} , is given by

$$\Delta\eta^{(\text{peak})} = \frac{2(n+2)}{n} \ln \left(\frac{k_n M_{jj}}{M_D} \right). \quad (62)$$

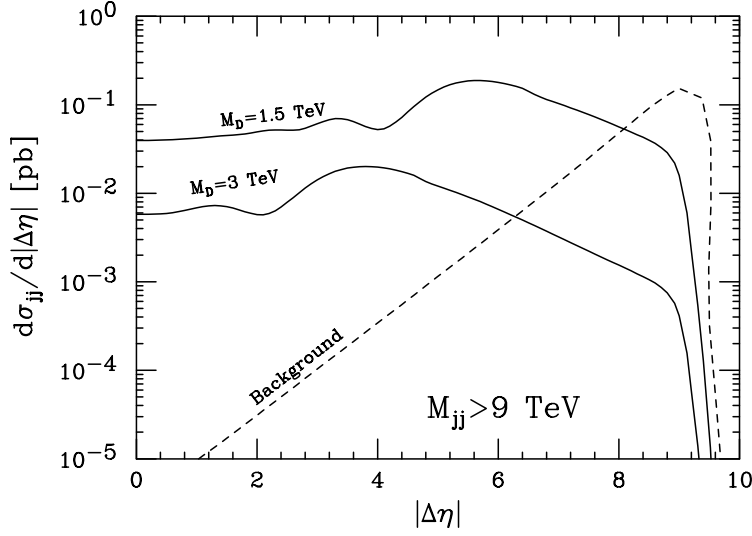


Figure 4: The di-jet differential cross section $d\sigma_{jj}/d|\Delta\eta|$ from eikonal gravity for $n = 6$, $M_{jj} > 9$ TeV, when both jets have $|\eta| < 5$ and $p_T > 100$ GeV, and for $M_D = 1.5$ TeV and 3 TeV. The dashed line is the expected rate from QCD.

The coefficients k_n can be obtained by numerically solving eq. (61) and are given by $k_{2,3,4,5,6} = 0.8, 0.9, 1.0, 1.2, 1.3$.

These peaks are a characteristic feature of the higher-dimensional gravitational force, and correspond to the diffraction pattern of the scattered particles. As discussed in sect. 2.3, higher-dimensional gravity, albeit leading to a force with infinite range, defines a length scale (b_c) in the quantum theory. A diffraction pattern emerges when $q \sim b_c^{-1}$ corresponding to the interference of the scattered waves in the region $b \sim b_c$. In the Coulomb case ($n = 0$), such a scale does not exist and therefore no diffractive pattern is produced.

The di-jet differential cross section $d\sigma_{jj}/d|\Delta\eta|$ is plotted in fig. 4 for $n = 6$, $M_{jj} > 9$ TeV and $M_D = 1.5$ TeV and 3 TeV. Since the parton-distribution functions decrease rapidly at higher M_{jj} , the value of M_{jj} in eq. (61) is well approximated by 9 TeV in this example. The first peaks are then calculated from eq. (62) to be at $\Delta\eta = 5.5$ ($M_D = 1.5$ TeV) and 3.7 ($M_D = 3$ TeV). The Monte Carlo integrated distributions have peaks that agree well with these numbers.

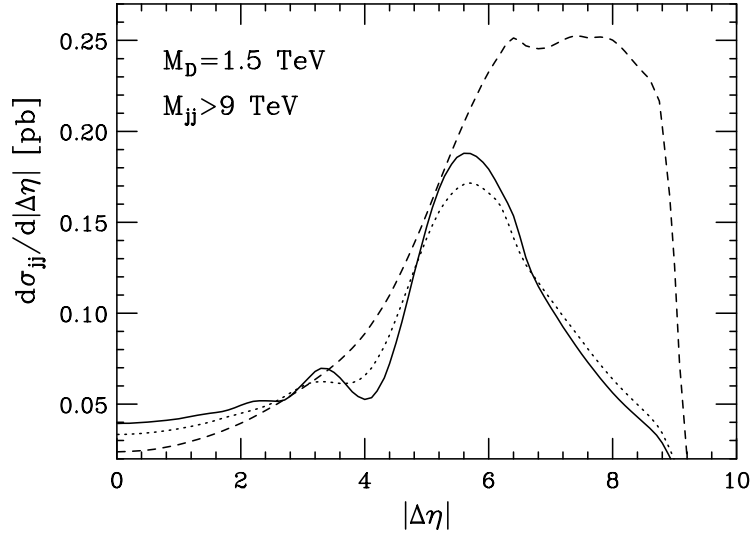


Figure 5: The di-jet differential cross section $d\sigma_{jj}/d|\Delta\eta|$ from eikonal gravity for $M_D = 1.5$ TeV and $n = 6$ (solid line), $n = 4$ (dotted line), and $n = 2$ (dashed line). We require $M_{jj} > 9$ TeV and that both jets have $|\eta| < 5$ and $p_T > 100$ GeV.

The same differential cross section is shown in fig. 5 for different values of n and for $M_D = 1.5$ TeV. For $n = 2$ the first peak is partly hidden by the logarithmic divergence for $\hat{t} \rightarrow 0$, and no structure after the first peak is visible. As n increases, the peaks become more evident. The study of the peak structure could be a feasible experimental technique to measure the number of extra spatial dimensions n . However, such a study can only be pursued with a full detector simulation, taking into account the rapidity and jet mass resolutions.

Since the two jets are experimentally indistinguishable, we have used $|\Delta\eta|$, instead of $\Delta\eta$, as the appropriate kinematical variable to plot. This means that the experimental signal considered here contains also contributions from scattering with large and negative $\Delta\eta$, which corresponds to partons colliding with large momentum transfer and retracing their path backwards. For the background, these effects are calculable and taken into account. However, the theoretical estimate of the signal at negative $\Delta\eta$ lies outside the range of validity of the eikonal approximation. Nevertheless, this is expected to be negligible and can

be safely ignored. Indeed, by dimensional arguments, the differential cross section for $t \rightarrow -s$ is estimated to be $d\sigma/dt \sim \pi R_S^2/s$, see eq. (30). When compared to the signal at small t ($d\sigma/dt \sim \pi b_c^4$), this gives a correction $\mathcal{O}[R_S^2/(sb_c^4)] \sim \mathcal{O}[(M_D^2/s)^{\frac{(n+2)^2}{n(n+1)}}]$, which is smaller than the terms we have neglected in our calculation, see eq. (43). Notice that this complication is unavoidable in the presence of identical colliding particles, since the amplitude is symmetric in t and u ($u = -s - t$).

Recalling our discussion of the corrections to the eikonal amplitude given in sect. 2.4, we notice that semiclassical corrections are indeed small. In the kinematical region of interest, the second term in eq. (43) amounts to less than 1% for $M_{jj} = 6M_D$ and $n < 6$ and less than 5% for $M_{jj} = 3M_D$ and $n < 6$, while the first term amounts to about 5% at $\Delta\eta = 3$. Gravitational radiation at $\Delta\eta = 3$ and $M_{jj} = 3M_D$ gives corrections of about 7% for $n = 2$ and 5% for $n = 6$, see eq. (45). Quantum gravity can however severely affect our signal. If the corresponding corrections had the form $(\lambda_P/b_c)^2$, then they would amount to 5% (6%) for $M_{jj} = 6M_D$ and $n = 2$ ($n = 6$) or to 20% (9%) for $M_{jj} = 3M_D$ and $n = 2$ ($n = 6$), and they would be under control. However, it is rather likely that the dynamics taming the ultraviolet behavior of gravity sets in at energies lower than M_D , enhancing these corrections. This is indeed the case of weakly-coupled strings, where in the previous estimate λ_P should be replaced by λ_S , giving an enhancement of M_D^2/M_S^2 . For instance, if the diffractive string production discussed in sect. 2.5 takes place, it will deplete the elastic channel at impact parameters smaller than b_D , which is typically very close to b_c , for values of M_D relevant for the LHC and for weakly-coupled strings. In this case, string production could be the discovery process at the LHC.

As is apparent from fig. 4, the background increases with $\Delta\eta$ faster than the signal, and so the best signal to background ratio is found at the smallest $\Delta\eta$. However, small $\Delta\eta$ are not in accord with the eikonal approximation. To stay within the acceptable kinematic range of the eikonal approximation we impose the condition $\Delta\eta > 3$, which is equivalent to $-\hat{t}/\hat{s} < 1/21$ and $\hat{\theta} < 25^\circ$. We then select a maximum value of $\Delta\eta$ in order to reject the background. In our study we make a simple universal choice $\Delta\eta < 4$, but in practice one could choose the maximum $\Delta\eta$ using only the criterion of retaining enough events to be detected. We want to

stress that this universal range of $\Delta\eta$ is chosen just for illustration, since its optimal choice depends on M_D . In particular, if M_D is below about 2 TeV, visible signals certainly can be obtained with a more stringent lower limit on $\Delta\eta$, therefore investigating a region of smaller scattering angles, where the eikonal approximation is even more accurate.

Furthermore, with the current computation technology of QCD, the dijet rate in our kinematic configuration is not a precision observable to compare with theory. This is especially true at large rapidity separation. However, our gravity signal can swamp the QCD expectation most notably at smaller rapidity separation, where the hard-scattering QCD rate is smaller and more reliably known. That is partly the reason why we choose for some plots to illustrate the gravity signal in the modest interval $3 < |\Delta\eta| < 4$.

At very large rapidity separation, the QCD dijet observable may be dominated by BFKL dynamics [35], in which case a decorrelation of the azimuthal angles of the two jets ensues [36]. Such a decorrelation is not expected in the color-singlet gravity signal. It may even be possible to use this to distinguish QCD from gravity. Similarly, the gravity signal is not expected to fill the central region with soft gluons, and the lack of this central jet activity could be an additional discriminating tool.

After having selected the range of $3 < |\Delta\eta| < 4$, we now show in fig. 6 the cross-section as a function of minimum jet-jet invariant mass cut for $M_D = 1.5$ TeV and 3 TeV. We plot results for all $M_{jj} \geq M_D$, but we recall that the eikonal approximation is valid only for $M_{jj}/M_D \gg 1$. This plot shows the important feature that the signal cross-section is flatter in M_{jj} than the background. This enables better signal to background for larger M_{jj} cuts, which is the preferred direction to go for eikonal approximation validity. Therefore, one should make the largest possible M_{jj} cut that still has a countable signal rate for a given luminosity.

Finally, in fig. 7 we plot the total integrated cross-section as a function of M_D for $M_{jj} > 3M_D$ (left panel) and $M_{jj} > 6M_D$ (right panel). We also have required $3 < |\Delta\eta| < 4$. The two solid lines correspond to $n = 6$ (upper line) and $n = 2$ (lower line). They are not far separated in this log plot. Figure 7 demonstrates several universal features. First, larger

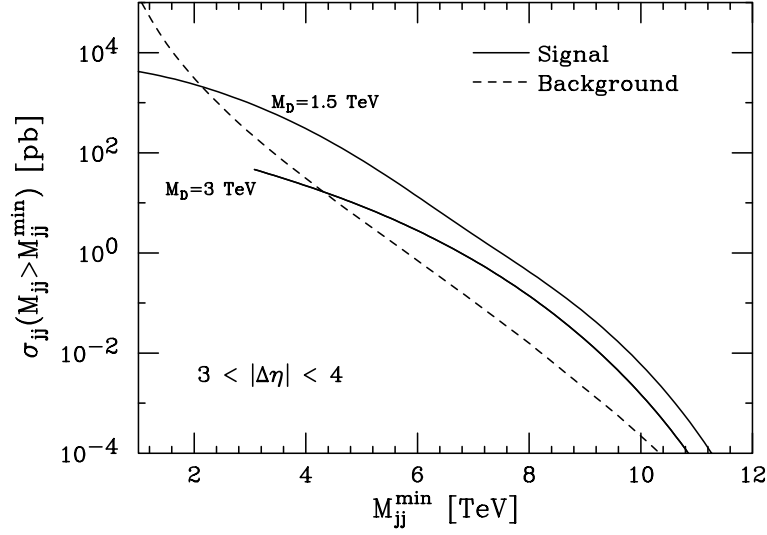


Figure 6: Total integrated di-jet cross-section for $3 < |\Delta\eta| < 4$, $n = 6$, and $M_{jj} > M_{jj}^{\min}$, when both jets have $|\eta| < 5$ and $p_T > 100$ GeV. Lines are plotted for $M_D = 1.5$ and 3 TeV. The eikonal approximation is reliable only where $M_{jj}/M_D \gg 1$. The expected QCD rate is given by the dashed line.

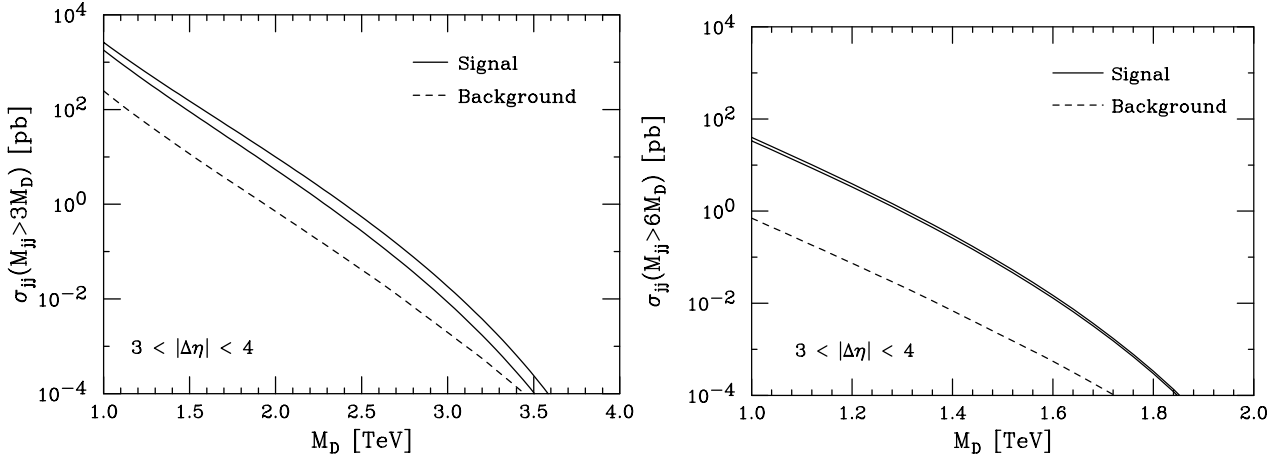


Figure 7: Total integrated di-jet cross-section for $3 < |\Delta\eta| < 4$, when both jets have $|\eta| < 5$ and $p_T > 100$ GeV, for (left panel) $M_{jj} > 3M_D$ and (right panel) $M_{jj} > 6M_D$. In each plot, the upper solid line is for $n = 6$ and the lower solid line is for $n = 2$. The dashed line is the expected QCD rate.

M_{jj}/M_D corresponds to a larger ratio of gravity signal to expected QCD rate, and to a more reliable applicability of the eikonal approximation. Larger M_{jj}/M_D also means less range of M_D probed at the LHC since parton luminosity drops rapidly as M_{jj} approaches the 14 TeV collider limit. In this paper, we will restrict our considerations to $M_{jj}/M_D > 3$ and so elastic scattering with M_D as large as 3.5 TeV can be tested with more than 10 events in 100 fb^{-1} . If we adopted the more conservative constraint $M_{jj}/M_D > 6$, the range of M_D where large and calculable signals are expected reduces to 1.8 TeV.

Before concluding this section on the LHC signatures, we recall that the eikonal jet-jet observable analyzed here is not the only transplanckian non-SM process. Black-hole production is also expected to be very large with a parton-parton production cross-section given approximately by $\sigma_{BH} \simeq \pi R_S^2$. As discussed earlier, this is just a dimensional-analysis estimate and reflects only the expectation that all collisions with impact parameter $b < R_S$ get absorbed into a black hole.

The description of the scattering process in terms of black-hole production is expected to be reliable only for black hole masses M_{BH} well above the D -dimensional gravity scale M_D . In the left panel of fig. 8 we plot the production cross-section as a function of minimum black-hole mass for $M_D = 1.5 \text{ TeV}$ and $M_D = 3 \text{ TeV}$. Although the lines are extended down to $M_{BH}^{\min} = M_D$, the reliable region is only $M_{BH}/M_D \gg 1$. The signatures of black holes are spectacular high-multiplicity events with almost no SM background [19]. Only a few events at very high invariant mass are needed to identify a signature. The right panel of fig. 8 shows the cross-section for black-hole production for $M_{BH} > 3M_D$ and $M_{BH} > 6M_D$. With an integrated luminosity of 100 fb^{-1} , a minimum of several events can be achieved for $M_D \simeq 3.5 \text{ TeV}$, if we require $M_{BH} > 3M_D$, or for $M_D \simeq 1.8 \text{ TeV}$ if $M_{BH} > 6M_D$. These values of M_D are nearly identical to what one can reach with the jet-jet observable discussed above. The combined search for black-hole production and small angle jet-jet events will be important for a full experimental characterization of the extra dimensions and for our ability to determine the underlying parameters of the theory.

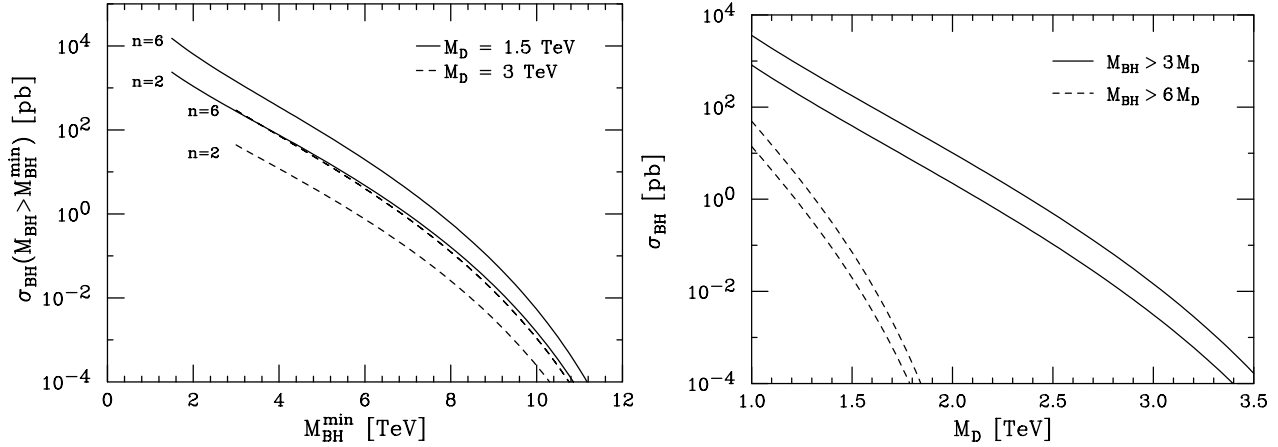


Figure 8: Black-hole production cross-section as a function of (left panel) minimum black-hole mass and (right panel) the gravity scale M_D .

3.2 Other Future Colliders

In addition to Tevatron upgrades and LHC, there are many colliders envisioned for the future. These include variants on the e^+e^- linear collider theme, the muon collider, and the very large hadron collider (VLHC). Observables associated with gravity are very sensitive to collider energies. The search for phenomena of almost all beyond-the-SM schemes is interested in higher and higher energies, but gravity is especially dependent on this progress. The reason is that either the rate increases at a high power of the collision energy if $s \ll M_D^2$, (*e.g.*, $\sigma \sim s^{n/2}/M_D^{n+2}$ for jet plus graviton signatures); or, well-chosen observables become calculable if $s \gg M_D^2$, (*e.g.*, in the case of eikonal gravity jet-jet production). Such calculability is taken for granted in many other beyond-the-SM frameworks. Either way, the highest energies attainable are important for increased understanding if low-scale gravity is correct.

We would therefore like to briefly discuss transplanckian collisions in the context of two of the highest energy colliders being considered in the not-too-distant future. The first is the VLHC [37], whose center-of-mass energy for proton-proton collisions is envisaged to be between 50 TeV and 200 TeV. Obviously the higher energy of this post-LHC machine will

be much more probing. Much of the analyses that we have described for the LHC would be applicable for VLHC analyses. By going to higher center-of-mass energies, we can gain in the range of sensitivity to M_D and, more importantly, we can study kinematical regions where quantum-gravity effects are expected to be smaller and the eikonal approximation becomes more trustworthy. For instance, by analysing dijet final states at the VLHC with invariant masses larger than 150 TeV, we can make quantum-gravity corrections (proportional to λ_S^2/b_c^2), for a fixed value of the string scale, about a factor of 200 (for $n = 2$) or 6 (for $n = 6$) smaller than their expected size in LHC experiments.

The other collider discussed at the highest currently imagined energy is CLIC [38], which is a two-beam e^+e^- linear collider design. Energies as high as $\sqrt{s} = 10$ TeV are being considered. Although such high-energy machines will have some spread in luminosity as a function of the center-of-mass energy, one still expects that approximately 1/4 of the beam luminosity will be within 1% of designed center-of-mass energy. With large gravity-induced cross sections (\sim pb or more) for all $M_D/\sqrt{s} \ll 1$, combined with relatively low background (\sim fb) and impressive luminosity design goals of 1 ab^{-1} , CLIC could certainly improve, verify and even discover the gravitational origin of beyond the SM signatures.

The maximum values of M_D that can be studied at CLIC in the gravitational deflection process (Bhabha scattering) are uniquely determined by the condition for validity of the eikonal approximation. For comparison, the condition equivalent to the one chosen in our LHC analysis is $M_D < \sqrt{s}/3$. Therefore, a linear collider with $\sqrt{s} = 10$ TeV could probe a parameter-space region, where theoretical calculations are reliable, which is very similar to the one that can be studied by LHC. However, the cleaner e^+e^- environment offer several advantages for precision tests and parameter determinations.

In fig. 9 we give one example of the signal and background distributions in the scattering angle θ for $M_D = 2$ TeV and $\sqrt{s} = 10$ TeV. Here θ is the scattering angle of the electron in the Bhabha process, and $\theta = 0$ indicates the electron going down the beam pipe undeflected by the collision. Notice that the SM background is completely insignificant as long as we exclude a small region around $\theta = 0$. This allows experimental studies of the cross section in a much more forward region than what is possible at the LHC.

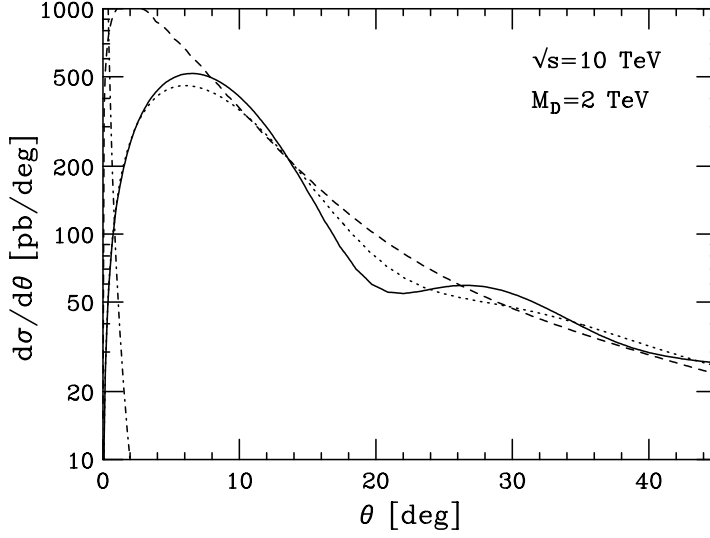


Figure 9: Angular distribution of the $e^+e^- \rightarrow e^+e^-$ signal for $M_D = 2 \text{ TeV}$ and $\sqrt{s} = 10 \text{ TeV}$. The solid line is for $n = 6$, the dotted for $n = 4$ and the dashed for $n = 2$. The almost-vertical dash-dotted line at the far left of the figure is the expected Bhabha scattering rate from the Standard Model.

The signal angular distribution is characterized by the peak structure encountered before, with minima and maxima described by the equation

$$\frac{1}{2} \left(1 - \tan^2 \frac{\theta}{2} \right) = - \frac{y}{|F_n(y)|} \frac{d|F_n(y)|}{dy} \bigg|_{y=b_c \sqrt{s} \sin \frac{\theta}{2}}. \quad (63)$$

The first peak is approximatlly given by

$$\theta^{(\text{peak})} \simeq \left(\frac{a_n M_D}{\sqrt{s}} \right)^{\frac{n+2}{n}}, \quad (64)$$

where a_n is a numerical coefficient with value $a_{2,3,4,5,6} = 0.9, 1.2, 1.1, 1.1, 1.0$. The $n = 6$ line (solid line) in fig. 9 is again the most telling line, since a careful measurement of the ups and downs of $d\sigma/d\theta$ would be hard to reproduce in another framework. Given the good energy and angular resolutions that can be achieved at a linear collider, CLIC could perform a much more precise study of the peak structure than what is feasible at the LHC.

Another advantage of CLIC is that unlike a pp collider, the scattering particles are distinguishable. This means that the calculable limit of $t \rightarrow 0$ (small angle scattering) is unambiguously identifiable. Recall that in the pp collider case, the case of partons glancing off each other at $\hat{t} \rightarrow 0$ was not distinguishable from partons bouncing backwards at large momentum transfer $\hat{t} \rightarrow -\hat{s}$. We argued that these non-calculable large momentum transfer contributions are negligible, but CLIC can test that assertion.

3.3 Comparison among Gravity Signals at the LHC

Let us conclude by comparing the various signals and experimental strategies for the discovery and the study of higher-dimensional gravitational interactions at the LHC. The two relevant parameters are the fundamental Planck mass M_D and the number of extra spatial dimensions n . We are tacitly assuming that the new dynamics of quantum gravity does not introduce a new mass scale smaller than M_D , or new phenomena in the relevant kinematical region. The searches for gravity signals at the LHC are classified in terms of three different kinematical regions.

Cisplanckian Region. This is the region in which the center-of-mass energy of the parton collision is smaller than the Planck mass, $\sqrt{\hat{s}} \ll M_D$. The theory can be described by an effective field-theory Lagrangian with non-renormalizable interactions, and the search for new contact interactions is an adequate experimental tool. However, the relations between the coefficients of the contact interactions and the fundamental gravity parameters is model dependent. In this region, the search for jet plus missing energy events is particularly interesting, because graviton emission can be reliably calculated with a perturbative expansion. The region [3] in which we can trust the effective theory for graviton emission is $M_D > 3.8$ TeV (for $n = 2$) or $M_D > 4.8$ TeV (for $n = 4$). LHC is sensitive to the graviton signal up to $M_D < 8.5$ TeV (for $n = 2$ and an integrated luminosity $\mathcal{L} = 100 \text{ fb}^{-1}$) or $M_D < 5.8$ TeV (for $n = 4$ and $\mathcal{L} = 100 \text{ fb}^{-1}$). In this window, LHC can perform a quantitative test of high-dimensional gravity in the cisplanckian region.

Planckian Region. This is the intermediate region $\sqrt{s} \simeq M_D$, where no experimental signals can be predicted without knowledge of the quantum-gravity theory. Signals from graviton emissions or elastic gravitational scattering are also present, but their rates cannot be reliably computed. New and unexpected phenomena will be the key to understand the underlying dynamics. Of course this is the region which will eventually yield the crucial experimental information.

Transplanckian Region. This is the region discussed in this paper, characterized by $\sqrt{s} \gg M_D$. The two experimental signals of interest in the transplanckian region are di-jet events (from elastic parton scattering) and black-hole production. Unfortunately, in the case of the LHC we are rather limited in energy for both processes. The actual conditions for calculability we have taken are $\sqrt{s} > 6M_D$ (in which the transplanckian region extends up to about 1.8 TeV) or the more optimistic $\sqrt{s} > 3M_D$ (in which the transplanckian region extends up to about 3.5 TeV). In both cases we are only marginally inside the transplanckian region since a complete separation between the quantum-gravity scale λ_P and the classical Schwarzschild radius R_S has not been fully reached. Therefore quantum-gravity contributions can potentially modify in a significant way both elastic scattering and black-hole formation. In our analysis, we have assumed that such contributions are small.

While the black-hole production cross section can only be estimated by dimensional analysis, the elastic cross section in the small-angle region can be computed as a perturbative expansion over controllable parameters. The elastic cross section is larger than the one for black-hole production. The observation of a cross section at finite angle growing with a power of s would be a clean signal that the high-energy dynamics of gravity has been detected. Given the highly characteristic events from black-hole evaporation, we expect negligible backgrounds for the black-hole events. As we have shown in this paper, the QCD background for di-jet events can be overcome by studying the distributions in di-jet invariant mass and rapidity separation. Therefore, the di-jet signal from the gravitational deflection of partons is not limited by the background. Its characteristic distributions can be used to test the gravitational nature of the interaction and to determine the parameters of the underlying theory.

Acknowledgments We wish to thank I. Antoniadis, J. Barbon, J. Bartels, S. Catani, P. Creminelli, A. De Roeck, R. Emparan, A. Ringwald, A. Strumia and G. Veneziano for useful discussions.

Appendix

In this appendix we collect some mathematical formulæ which are useful to reproduce computations presented in this paper. The Bessel functions $J_n(x)$ have the following series expansions

$$J_n(x) = \sum_{k=0}^{\infty} \frac{(-)^k (x/2)^{2k+n}}{k! \Gamma(k+n+1)}, \quad (65)$$

$$J_n(x) = \sqrt{\frac{2}{\pi x}} \left\{ \cos \left[x - (2n+1) \frac{\pi}{4} \right] - \frac{4n^2-1}{8x} \sin \left[x - (2n+1) \frac{\pi}{4} \right] + \mathcal{O} \left(\frac{1}{x^2} \right) \right\}. \quad (66)$$

Some useful integrals are

$$\int d^n y \, e^{i\vec{x} \cdot \vec{y}} f(y) = \frac{(2\pi)^{\frac{n}{2}}}{x^{\frac{n}{2}-1}} \int_0^\infty dy \, y^{\frac{n}{2}} J_{\frac{n}{2}-1}(xy) f(y), \quad (67)$$

for a generic function f , and with $x \equiv |\vec{x}|$, $y \equiv |\vec{y}|$.

$$\int_0^\infty dx \, x^a J_n(x) = 2^a \Gamma \left(\frac{1+n+a}{2} \right) / \Gamma \left(\frac{1+n-a}{2} \right). \quad (68)$$

$$\int_0^\infty dx \, x^{a-1} (e^{ix^{-n}} - 1) = -\frac{1}{a} \Gamma \left(1 - \frac{a}{n} \right) e^{-\frac{i\pi a}{2n}}. \quad (69)$$

$$\int_0^\epsilon dx \, x^a e^{ix^{-n}} = \frac{\epsilon^{a+1+n}}{n} e^{i(\epsilon^{-n} + \frac{\pi}{2})} [1 + \mathcal{O}(\epsilon^n)] \quad \text{for } a > -n-1. \quad (70)$$

References

- [1] N. Arkani-Hamed, S. Dimopoulos and G. R. Dvali, Phys. Lett. B **429**, 263 (1998).
- [2] L. Randall and R. Sundrum, Phys. Rev. Lett. **83**, 3370 (1999).

- [3] G. F. Giudice, R. Rattazzi and J. D. Wells, Nucl. Phys. B **544**, 3 (1999).
- [4] E. A. Mirabelli, M. Perelstein and M. E. Peskin, Phys. Rev. Lett. **82**, 2236 (1999).
- [5] T. Han, J. D. Lykken and R. J. Zhang, Phys. Rev. D **59**, 105006 (1999); J. L. Hewett, Phys. Rev. Lett. **82**, 4765 (1999).
- [6] S. Cullen, M. Perelstein and M. E. Peskin, Phys. Rev. D **62**, 055012 (2000); E. Dudas and J. Mourad, Nucl. Phys. B **575**, 3 (2000); E. Accomando, I. Antoniadis and K. Benakli, Nucl. Phys. B **579**, 3 (2000);
- [7] R. C. Myers and M. J. Perry, Annals Phys. **172**, 304 (1986).
- [8] H. Cheng and T.T. Wu, Phys. Rev. Lett. **22**, 666 (1969); H. Abarbanel and C. Itzykson, Phys. Rev. Lett. **23**, 53 (1969); M. Levy and J. Sucher, Phys. Rev. **186**, 1656 (1969).
- [9] D. Kabat and M. Ortiz, Nucl. Phys. B **388**, 570 (1992); D. Kabat, Comments Nucl. Part. Phys. **20**, 325 (1992).
- [10] D. Amati, M. Ciafaloni and G. Veneziano, Phys. Lett. B **197**, 81 (1987); Int. J. Mod. Phys. A **3**, 1615 (1988); Nucl. Phys. B **347**, 550 (1990); Nucl. Phys. B **403**, 707 (1993).
- [11] I. J. Muzinich and M. Soldate, Phys. Rev. D **37**, 359 (1988).
- [12] I. Y. Aref'eva, K. S. Viswanathan and I. V. Volovich, Nucl. Phys. B **452**, 346 (1995).
- [13] G. 't Hooft, Phys. Lett. B **198**, 61 (1987).
- [14] P. C. Aichelburg and R. U. Sexl, Gen. Rel. Grav. **2**, 303 (1971).
- [15] H. Verlinde and E. Verlinde, Nucl. Phys. B **371**, 246 (1992).
- [16] D. Amati, M. Ciafaloni and G. Veneziano, Phys. Lett. B **289**, 87 (1992).
- [17] R. Emparan, Phys. Rev. D **64**, 024025 (2001); R. Emparan, M. Masip and R. Rattazzi, hep-ph/0109287.

- [18] S. Nussinov and R. Shrock, Phys. Rev. D **64**, 047702 (2001).
- [19] S. B. Giddings and S. Thomas, hep-ph/0106219; S. Dimopoulos and G. Landsberg, Phys. Rev. Lett. **87**, 161602 (2001); S. B. Giddings, hep-ph/0110127.
- [20] K. Cheung, hep-ph/0110163; A. Ringwald and H. Tu, hep-ph/0111042; T. G. Rizzo, hep-ph/0111230.
- [21] M. B. Voloshin, Phys. Lett. B **518**, 137 (2001); hep-ph/0111099.
- [22] S. Dimopoulos and R. Emparan, hep-ph/0108060.
- [23] L. D. Landau and E.M. Lifshitz, Quantum Mechanics, vol. 3 of *Course of Theoretical Physics*.
- [24] D. J. Gross and P. F. Mende, Phys. Lett. B **197**, 129 (1987); Nucl. Phys. B **303**, 407 (1988).
- [25] I. Antoniadis, N. Arkani-Hamed, S. Dimopoulos and G. R. Dvali, Phys. Lett. B **436**, 257 (1998).
- [26] I. Antoniadis, K. Benakli and A. Laugier, JHEP **0105**, 044 (2001).
- [27] R. Contino, L. Pilo, R. Rattazzi and A. Strumia, JHEP **0106**, 005 (2001).
- [28] P. F. Mende and H. Ooguri, Nucl. Phys. B **339**, 641 (1990).
- [29] K. Oda and N. Okada, hep-ph/0111298.
- [30] R. Sundrum, Phys. Rev. D **59**, 085009 (1999).
- [31] C. Charmousis, R. Emparan and R. Gregory, JHEP **0105**, 026 (2001).
- [32] H. L. Lai *et al.*, Phys. Rev. D **51**, 4763 (1995).
- [33] M. Gluck, E. Reya and A. Vogt, Z. Phys. C **67**, 433 (1995).
- [34] T. Sjostrand, L. Lonnblad and S. Mrenna, hep-ph/0108264.

- [35] A. H. Mueller and H. Navelet, Nucl. Phys. B **282**, 727 (1987); L. H. Orr and W. J. Stirling, Phys. Lett. B **436**, 372 (1998).
- [36] V. Del Duca and C. R. Schmidt, Phys. Rev. D **49**, 4510 (1994); Phys. Rev. D **51**, 2150 (1995); W. J. Stirling, Nucl. Phys. B **423**, 56 (1994); L. H. Orr and W. J. Stirling, Phys. Rev. D **56**, 5875 (1997).
- [37] See <http://www-ap.fnal.gov/VLHC/>.
- [38] See <http://clicphysics.web.cern.ch/CLICphysics/>.